

1 **Application and assessment of a membrane-based pCO<sub>2</sub> sensor under field and laboratory**  
2 **conditions**

3 Zong-Pei Jiang<sup>\*1,2</sup>, David J. Hydes<sup>1</sup>, Sue E. Hartman<sup>1</sup>, Mark C. Hartman<sup>1</sup>, Jon M. Campbell<sup>1</sup>,  
4 Bruce D. Johnson<sup>3</sup>, Bryan Schofield<sup>3</sup>, Daniela Turk<sup>4,5</sup>, Douglas Wallace<sup>4</sup>, William Burt<sup>4</sup>, Helmuth  
5 Thomas<sup>4</sup>, Cathy Cosca<sup>6</sup>, Richard Feely<sup>6</sup>

6 <sup>1</sup> National Oceanography Centre Southampton, European Way, Southampton, UK

7 <sup>2</sup> State Key Laboratory of Marine Environmental Science, Xiamen University, Xiamen, China

8 <sup>3</sup> ProOceanus Systems Inc., Bridgewater, Nova Scotia, Canada.

9 <sup>4</sup> Department of Oceanography, Dalhousie University, Halifax, NS, Canada

10 <sup>5</sup> Lamont-Doherty Earth Observatory, Columbia University, NY, USA

11 <sup>6</sup> Pacific Marine Environmental Lab, NOAA, Seattle, WA, USA

12

13 \*Corresponding author: Zong-Pei Jiang

14 National Oceanography Centre Southampton, University of Southampton

15 European Way, Southampton, United Kingdom, SO14 3ZH

16

17 Running head: Assessment of a membrane-based NDIR pCO<sub>2</sub> sensor

18

19 **Acknowledgment**

20 The Swire Charitable Trust and the Swire Education Trust are gratefully acknowledged for  
21 funding the Swire NOCS Ocean Monitoring System (SNOMS) project and the scholarship for  
22 Zong-Pei Jiang's PhD study. The Swire Group Company China Navigation and the crews on the  
23 *MV Pacific Celebes* are to be thanked for supporting the operation of the SNOMS project. Dave  
24 Childs provided invaluable analysis of the salinity samples at NOCS. At the Institute of Ocean  
25 Science in Canada, Marty Davelaar, Jim Christian and Kyle Davidson helped with sample pickups  
26 and joined in the SNOMS sample processing exercise. We gratefully thank Jim Eddington, Emily  
27 Chua, Claire Normandeau, Trina Whitsitt and Douglas Schillinger during the Aquatron tests at  
28 Dalhousie University. We also thank the support from Richard Lampitt, Kate Larkin, Maureen  
29 Pagnani, Thanos Gkritzalis on the sensor deployment and maintenance at the PAP site. Wei-Jun  
30 Cai is thanked for the helpful discussion on the organic alkalinity. We also thank Mike  
31 DeGrandpre and Wiley Evans for their helpful suggestions on improving this paper.

32

33 **Abstract**

34 The principle, application and assessment of the membrane-based ProOceanus CO<sub>2</sub>-Pro<sup>TM</sup> sensor  
35 for partial pressure of CO<sub>2</sub> (pCO<sub>2</sub>) are presented. The performance of the sensor is evaluated  
36 extensively under field and laboratory conditions by comparing the sensor outputs with references  
37 of direct measurements from calibrated pCO<sub>2</sub> measuring systems and the thermodynamic  
38 carbonate calculation from discrete samples. Under stable laboratory condition, the sensor agreed  
39 with a calibrated water-air equilibrators system at  $-3.0 \pm 4.4 \mu\text{atm}$  during a 2-month  
40 intercomparison experiment. When applied in field deployments, the larger differences between  
41 measurements and the calculated pCO<sub>2</sub> references ( $6.4 \pm 12.3 \mu\text{atm}$  on a ship of opportunity and  
42  $8.7 \pm 14.1 \mu\text{atm}$  on a mooring) are related not only to sensor error, but also to the uncertainties of  
43 the references and the comparison process, as well as changes in the working environments of the  
44 sensor. When corrected against references, the overall uncertainties of the sensor results are  
45 largely determined by those of the pCO<sub>2</sub> references ( $\pm 2$  and  $\pm 8 \mu\text{atm}$  for direct measurements  
46 and calculated pCO<sub>2</sub> respectively). Our study suggests accuracy of the sensor can be affected by  
47 temperature fluctuations of the detector optical cell and calibration error. These problems have  
48 been addressed in more recent models of the instrument through improving detector temperature  
49 control and through using more accurate standard gases. Another interesting result in our  
50 laboratory test is the unexpected change in alkalinity which results in significant underestimation  
51 in the pCO<sub>2</sub> calculation as compared to the direct measurement (up to  $90 \mu\text{atm}$ ).

52

53 **Introduction**

54 The knowledge of surface ocean CO<sub>2</sub> variability is important for understanding the marine carbon  
55 cycle and its future response to the absorption of anthropogenic CO<sub>2</sub> (Doney et al. 2009). In the  
56 past few decades, high-accuracy seawater pCO<sub>2</sub> measuring systems (Körtzinger et al. 1996;  
57 Dickson et al. 2007; Pierrot et al. 2009) have been widely used on research vessels providing high  
58 quality pCO<sub>2</sub> data, which leads to the generation of a global atlas of the surface ocean pCO<sub>2</sub>  
59 (Surface Ocean CO<sub>2</sub> Atlas, <http://www.socat.info/>, Bakker et al. 2013) and CO<sub>2</sub> flux  
60 (Takahashi et al. 2009). However, there is still a lack of data from large areas of the globe,  
61 especially in the shelf seas, Southern Ocean, and southern-hemisphere subtropical gyres (Doney et  
62 al. 2009). Moreover, changes in seawater pCO<sub>2</sub> can occur on timescales from daily (Degrandpre et  
63 al. 1998; Yates et al. 2007; Dai et al. 2009; Turk et al. 2013) to seasonal and interannual (Bates  
64 2002, 2007; Watson et al. 2009; Jiang et al. 2013), especially in the dynamic coastal environments  
65 (Borges and Frankignoulle 1999; Thomas and Schneider 1999; De La Paz et al. 2008; Turk et al.  
66 2010; Jiang et al. 2011). Observations with sufficient temporal and spatial resolution are thus  
67 needed for a better understanding of the controlling mechanism of pCO<sub>2</sub> variability in different  
68 regions and for a more reliable CO<sub>2</sub> flux estimation.

69 In addition to the traditional shipboard measuring system (e. g. the General Oceanics pCO<sub>2</sub>  
70 measuring system) , there are emerging techniques to develop autonomous pCO<sub>2</sub> sensors. As  
71 summarized in Table 1, these sensors generally follow the same basic concept based on the  
72 measurement of a gas or indicator solution that is in equilibrium with the seawater to be  
73 determined. The equilibrium state can be reached by using water-gas equilibrators where the gas is  
74 directly in contact with the seawater, or via gas permeable interfaces such as polydimethylsiloxane

75 (PDMS) or polytetrafluoroethene (PTFE) membrane. The equilibrated gas can be measured by a  
76 non-dispersive infrared (NDIR) spectrometry, while the equilibrated indicator solution can be  
77 determined by electrode, fluorescence or spectrophotometric methods (Table 1). For these  
78 reagent-based fibre optic chemical sensors (Goyet et al. 1992; Degrandpre 1993; Lefèvre et al.  
79 1993; Degrandpre et al. 1995), improvements have been made by using multi-wavelength  
80 detection and long pathlength liquid-core waveguides for better precision and accuracy  
81 (Degrandpre et al. 1999; Wang et al. 2002; Wang et al. 2003; Nakano et al. 2006; Lu et al. 2008).

82 Evolving sensor technology has enabled cost-effective  $p\text{CO}_2$  measurements to be made on  
83 various platforms such as ship of opportunity (SOO), buoy and mooring, glider, profiling float and  
84 autonomous underwater vehicle (Degrandpre et al. 1998; Nakano et al. 2006; Nemoto et al. 2009;  
85 Willcox et al. 2009; Fiedler et al. 2012; Saderne et al. 2013).

86 In this paper, we describe the principle and design of a membrane-based NDIR  $p\text{CO}_2$  sensor  
87 (ProOceanus  $\text{CO}_2\text{-Pro}^{\text{TM}}$ , hereafter referred to as  $\text{CO}_2\text{-Pro}$ ). The sensor's functionality, reliability  
88 and accuracy are evaluated under various situations including: a 16-day coastal mooring  
89 deployment test adjacent to a coral reef in Hawaii (October to November 2009), shipboard  
90 underway mapping on a SOO (October 2009 to March 2012), intercomparison with a calibrated  
91 water-gas equilibrator system in the Aquatron Laboratory at Dalhousie University (May to  
92 September 2012) and long-term open-ocean mooring deployment in the Northeast Atlantic (June  
93 2010 to July 2012). The performance of the  $\text{CO}_2\text{-Pro}$  is assessed by comparing the sensor outputs  
94 against two kinds of reference: (1) the thermodynamic carbonate calculation of  $p\text{CO}_2$  from the  
95 determinations of dissolved inorganic carbon (DIC), total alkalinity (TA), and pH from discrete  
96 samples; (2) direct measurements by the traditional water-gas equilibrator NDIR systems which

97 are regularly calibrated against standard gases. The advantages and limitations of the CO<sub>2</sub>-Pro are  
98 summarized and the recent improvements of the instrument are introduced.

## 99 **Materials and Procedures**

### 100 *Principle of the CO<sub>2</sub>-Pro*

101 The CO<sub>2</sub>-Pro is designed as a light-weight, compact, plug and play, versatile instrument for pCO<sub>2</sub>  
102 measurements on moorings, drifters and profilers, in underway mode and in laboratories. As  
103 shown in Figure 1, the sensor is fitted with an equilibrator composed of a gas permeable PDMS  
104 membrane (other membrane materials are also available) and an internal detection loop with a  
105 NDIR detector based on a highly modified PPSystems SBA-4 CO<sub>2</sub> analyzer. The patented gas  
106 transfer interface of the equilibrator features a tubular design, through which the equilibration  
107 between the surrounding water and the internal gas stream can be achieved. Copper wire is wound  
108 round the tube to inhibit the potential for bio-film formation and the equilibrator is protected from  
109 physical damage by an end-cap. An associated Seabird Electronics SBE 5M submersible pump  
110 flows water past the outer surface of the equilibrator membrane to accelerate the equilibration.  
111 The response time, i.e. the time for the membrane to reduce the perturbation in pCO<sub>2</sub> by a factor  
112 of 1/e, is typically 2 minutes depending on the pumping rate. NDIR measurement on the  
113 equilibrated internal gas is taken at a wavelength of 4.26 μm at a controlled optical cell  
114 temperature (30, 40 or 55°C). In addition, temperature, pressure and humidity of the internal gas  
115 are determined to correct the CO<sub>2</sub> measurement. Further detailed specifications of the CO<sub>2</sub>-Pro can  
116 be found at the company's website <http://www.pro-oceanus.com/co2-pro.php>.

117 When the sensor is turned on, the optical cell of the detector warms up and then stabilizes at the  
118 temperature set point. A zero point calibration (ZPC) is then carried out to provide a zero-CO<sub>2</sub>

119 baseline ( $C_{zero}$ ) for the subsequent NDIR absorption measurement. This is done by circulating the  
120 internal gas through a CO<sub>2</sub> absorption chamber containing soda lime or Ascarite (flow path: valve  
121 2 - circulation pump - optical cell - valve 3 - absorption chamber - valve 2, Fig. 1). When the ZPC  
122 finishes, the solenoid valves 2 and 3 are activated to circulate the internal gas around a closed  
123 circuit connecting the equilibrator and detector (flow path: valve 2 - circulation pump - optical cell  
124 - valve 3 - valve 4 - equilibrator - valve 1- valve 2, Fig. 1). The inferred signal of the internal gas  
125 ( $C_{meas}$ ) is measured to calculate the absorbance ( $\epsilon = C_{meas} / C_{zero}$ ) and CO<sub>2</sub> concentration. Once the  
126 internal gas is equilibrated with the water surrounding the equilibrator (typically 10-15 minutes  
127 after the ZPC), the seawater CO<sub>2</sub> concentration can be determined. The CO<sub>2</sub>-Pro features a  
128 programmable regular automatic ZPC function to correct the detector drift which can be caused by  
129 contamination of the optical cell, optical source ageing and changes in detector sensitivity.

130 Each CO<sub>2</sub>-Pro is factory calibrated at a known optical cell temperature and pressure against 5  
131 standard gasses with xCO<sub>2</sub> (mole fraction of CO<sub>2</sub> in dry air) spanning from 0 to 600 ppm (other  
132 calibration ranges are also available). The calibration equation is obtained by a three-segment  
133 least-squares fitting to a quadratic equation between  $\epsilon$  and xCO<sub>2</sub>. This equation is subsequently  
134 tested by measuring a further three known mixtures of CO<sub>2</sub>. While the calibration equation  
135 provides a raw xCO<sub>2</sub> from the inferred measurement, empirical corrections are applied to account  
136 for the differences of conditions between calibration and measurement (temperature, pressure,  
137 water vapour). As the actual measurement is made on gas which is nearly saturated with water  
138 vapour, the output of CO<sub>2</sub>-Pro is the mole fraction of CO<sub>2</sub> in wet air (wCO<sub>2</sub>, ppm) and pCO<sub>2</sub> in the  
139 measured water is obtained by:  $pCO_2 = wCO_2 * P_{wet}$ , where  $P_{wet}$  is the measured total pressure of  
140 the internal gas which includes water vapour pressure.

141 *ACT coastal mooring test*

142 The application of the CO<sub>2</sub>-Pro in coastal mooring measurement was previously tested in a  
143 demonstration project organized by the Alliance for Coastal Technologies (ACT)  
144 (<http://www.act-us.info/evaluations.php#pco2>). During October to November 2009, a CO<sub>2</sub>-Pro  
145 was mounted on a surface mooring and deployed at a fixed depth of 1 m close to a shallow  
146 sub-tropical coral reef in Kaneohe Bay, Hawaii. Continual measurements were made by the  
147 CO<sub>2</sub>-Pro on an hourly basis and the results were compared with the reference pCO<sub>2</sub> calculated  
148 from discrete samples. pH and TA of these samples were measured spectrophotometrically using  
149 meta-cresol purple and bromo-cresol green as indicators, respectively (Dickson et al. 2007). Both  
150 measurements were calibrated against the Certified Reference Material (CRM) from Scripps  
151 Institution of Oceanography. The accuracy of the pH measurement was estimated to be 0.005 and  
152 the standard deviation (SD) of repeated TA measurements was 1.9 μmol kg<sup>-1</sup> (ACT 2009b).  
153 Details of the deployment, measurements, calculation and quality control were documented by  
154 ACT (2009a, b).

155 *SNOMS underway measurements*

156 From June 2007 to March 2012, CO<sub>2</sub>-Pro sensors were used for continuous shipboard underway  
157 measurement in the operation of a SOO-based measuring system (referred to as SNOMS) on the  
158 *MV Pacific Celebes* (Hydes et al. 2013). For these measurements a CO<sub>2</sub>-Pro was mounted in a  
159 45-litre flow-through pressure tank, together with other sensors for temperature, conductivity,  
160 dissolved oxygen and total dissolved gas pressure. To adapt it to the SNOMS tank, the protecting  
161 end-cap and the associated water pump of the CO<sub>2</sub>-Pro were removed. The gas transfer interface  
162 was thus directly exposed to the seawater for pCO<sub>2</sub> measurement, which also enabled direct



163 cleaning of the membrane surface. The SNOMS tank was fed at a flow rate of  $28 \pm 2$  litres  
164  $\text{minute}^{-1}$  by a branch of the non-toxic seawater being pumped to the ship's fresh water generator.  
165 This water supply was routinely turned off in shallow and potentially turbid water, thereby  
166 preventing sedimentation in the tank and contamination of the membrane of the CO<sub>2</sub>-Pro. At each  
167 port, the tank was opened and the CO<sub>2</sub>-Pro membrane was cleaned by hosing it down with fresh  
168 water.

169 The CO<sub>2</sub>-Pro was continuously working when the SNOMS system was in operation. The  
170 frequency of the automatic ZPC was set to be 6 hours, and the 15 minutes of data after each ZPC  
171 (when the internal gas was re-equilibrating with the water) was discarded. In order to account for  
172 the difference between the water temperature in the tank ( $T_{\text{tank}}$ ) and that in the surface ocean, an  
173 insulated Seabird 48 hull-contact temperature sensor was used to monitor the sea surface  
174 temperature (SST). The time lag between SST and  $T_{\text{tank}}$  was estimated to be ~30 seconds. By  
175 considering the temperature effect on pCO<sub>2</sub> (Takahashi et al. 1993), the tank water pCO<sub>2</sub>  
176 measured by CO<sub>2</sub>-Pro ( $p\text{CO}_{2,\text{Pro}}$ ) was corrected to the sea surface condition:  $p\text{CO}_{2,\text{SST}} = p\text{CO}_{2,\text{Pro}} * \text{exp}[0.0423 * (\text{SST} - T_{\text{tank}})]$   
177 The likely accuracy of SST from the hull measurement is 0.1 °C (Beggs  
178 et al. 2012), which results in an uncertainty of ~1.5  $\mu\text{atm}$  in converting  $p\text{CO}_{2,\text{Pro}}$  to  $p\text{CO}_{2,\text{SST}}$ .

179 In addition to the underway measurements, discrete samples were collected by the ship's  
180 engineers for the determination of DIC and TA. These samples were shipped to the National  
181 Oceanography Centre, Southampton (NOCS) and were measured under stable laboratory  
182 conditions. The CRM-calibrated measurements of DIC and TA were carried out using a VINDTA  
183 3C (Marianda, Germany). Repeat measurements on pooled samples were undertaken before

184 sample analysis each day ( $n > 3$ ), these suggested a precision better than  $\pm 2 \mu\text{mol kg}^{-1}$  for DIC and  
185  $\pm 1.5 \mu\text{mol kg}^{-1}$  for TA respectively.

### 186 *The Aquatron laboratory test*

187 After the operation on the *MV Pacific Celebes*, a controlled test of the CO<sub>2</sub>-Pro as a part of the  
188 SNOMS tank was carried out in the Aquatron Laboratory at Dalhousie University during May to  
189 September 2012. To carry out this test, a two cubic metre open tank (referred to as the Aquatron  
190 tank) was set up beside the SNOMS tank. The two tanks were filled with sand-bed filtered  
191 seawater pumped from an adjacent harbour (estuary) on 23 May. The water was continuously  
192 pumped in a circuit between the two tanks with a turnover time of about 2 hours. The pCO<sub>2</sub> of the  
193 tank water was monitored by the CO<sub>2</sub>-Pro in the SNOMS system which operated in a similar way  
194 as on the *MV Pacific Celebes*. After a stabilization period of ~50 days when the pCO<sub>2</sub> reached a  
195 relatively constant range, another pCO<sub>2</sub> measuring system (referred to as the NOIZ system) was  
196 set up in the Aquatron tank for a side-by-side comparison with the CO<sub>2</sub>-Pro. In order to control  
197 pCO<sub>2</sub> to ocean values during the two-month intercomparison exercise (13 July to 11 September),  
198 a simple system was developed to bubble CO<sub>2</sub>-free gas (laboratory air passing through a cartridge  
199 filled with soda lime) into the Aquatron tank on three occasions (started on 10 July, 2 August and  
200 31 August, Fig. 6).

201 The NOIZ system consisted of a bubble type water-gas equilibrator and a Licor 7000 NDIR  
202 detector (Körtzinger et al. 1996). The equilibrator was mounted on the Aquatron tank and its  
203 lower part was submerged in the water to minimize the temperature difference between the tank  
204 water and that in the equilibrator. The detector was calibrated every a few days with zero CO<sub>2</sub>  
205 concentration nitrogen gas and an air mixture calibrated with National Oceanic and Atmospheric

206 Administration (NOAA) standard gas before 27 August 2012. After that, the calibration directly  
207 used a NOAA-supplied standard gas with an uncertainty of  $\pm 1$  ppm. No shift could be identified  
208 in the calibration when calibration gasses were changed. The accuracy of the  $p\text{CO}_2$  measured by  
209 the NOIZ system was estimated to be within  $2 \mu\text{atm}$ .

210 In addition to the  $p\text{CO}_2$  measurements, discrete samples for DIC and TA were collected  
211 throughout the test on a daily basis. Nutrient samples were collected from 5 June onwards for  
212 determination of nitrate, silicate, phosphate and ammonia (Whitledge et al. 1981). To compensate  
213 for water loss due to sampling and evaporation, the Aquatron tank was topped up every 4-7 day  
214 with newly pumped water. Although this water was pumped from the same location, it may  
215 have different properties compared to the original tank water due to the temporal variability at the  
216 sampling site. However, these top up events only had a minor influence on the chemical  
217 concentrations of the tank water because of the relatively small volumes added (0.2-3% of the  
218 total volume of the Aquatron tank). One exception was a substantial top up on 7 August (35%  
219 of the total volume) because of a large drainage from the sampling tube, which significantly  
220 changed the properties of the tank water (see the results section below).

### 221 *Long-term in situ operation on the PAP mooring*

222 Since June 2010, the  $\text{CO}_2$ -Pro was used for long-term in situ deployment at the Porcupine Abyssal  
223 Plain site (PAP,  $49^\circ\text{N}$   $16.5^\circ\text{W}$ , 4800 m water depth) which is the longest running  
224 multidisciplinary observatory in the Northeast Atlantic (Hartman et al. 2012). It was deployed on a  
225 sensor frame at a fixed depth of 30 m together with other autonomous sensors for temperature,  
226 salinity, chlorophyll-a fluorescence and nitrate. All these sensors were controlled by a hub  
227 controller which communicated with NOCS via satellite in near real-time. The  $\text{CO}_2$ -Pro was

228 powered by the solar panels on the mooring and its measurement frequency and the time length  
229 for each measurement could be changed remotely.

### 230 *The carbonate system calculation*

231 The marine carbonate system can be characterized from any two of the four parameters: DIC, TA,  
232 pCO<sub>2</sub> and pH (Zeebe and Wolf-Gladrow 2001). In this study, the Excel program “CO2SYS”  
233 (Pierrot et al. 2006) was used for the carbonate calculations. The dissociation constants of  
234 carbonic acid (pK<sub>1</sub> and pK<sub>2</sub>) determined in real seawater by Millero et al. (2006) are in good  
235 agreement with previous measurements (Mehrbach et al. 1973; Mojica Prieto and Millero 2002),  
236 and are more reliable than those measured in artificial seawater (Millero et al. 2006). Therefore,  
237 we chose to use the constants of Millero et al. (2006) in our CO2SYS calculations. The sulphuric  
238 dissociation was chosen as Dickson (1990) and the total boron formulation was selected as Lee et  
239 al. (2010). In this study, pCO<sub>2</sub> was calculated either from the combination of pH and TA (ACT  
240 test) or DIC and TA (SNOMS and Aquatron test). The uncertainty of the pCO<sub>2</sub> calculation comes  
241 from inaccuracies in the thermodynamic dissociation constants (mainly pK<sub>1</sub> and pK<sub>2</sub>) and the  
242 experimental measurements of the variables used for calculation (Millero et al. 2006). As shown  
243 in Table, 2, the various sources of uncertainties associated with the carbonate calculation yield  
244 uncertainties in the calculated pCO<sub>2</sub> which are estimated to be ± 7.5 µatm for the ACT test (ACT  
245 2009a, b), ± 8.1 µatm for the SNOMS operation and ± 9.9 µatm for the Aquatron test within the  
246 measured pCO<sub>2</sub> ranges, respectively.

### 247 **Assessment**

#### 248 *Results of the ACT coastal mooring test*

249 The results of the ACT mooring test have been reported by ACT (2009a) and are briefly  
250 summarized here. During the 16-day continuous measurement in Kaneohe Bay, nearly 100% of  
251 the data were retrieved except for the data gaps during calibration cycles. The hourly time series  
252 data from the CO<sub>2</sub>-Pro (pCO<sub>2,Pro</sub> in Fig. 2A, 280-840 μatm) shows a significantly greater dynamic  
253 range compared to the values calculated from pH and TA (pCO<sub>2,pHTA</sub>, 314-608 μatm). The higher  
254 measurement frequency of the CO<sub>2</sub>-Pro thus better characterized the short-term variability of  
255 pCO<sub>2</sub> that was mainly caused by the strong biological activities of the adjacent coral reef system.  
256 The 5-minute averages of the sensor outputs bracketing the time of discrete sample collection  
257 were compared to the calculated pCO<sub>2,pHTA</sub> in Figure 2. The mean and SD of the differences  
258 between the paired pCO<sub>2,Pro</sub> and pCO<sub>2,pHTA</sub> measurements ( $\delta pCO_2 = pCO_{2,Pro} - pCO_{2,pHTA}$ , Fig. 2C,  
259  $\delta pCO_2$  refers to the difference between the raw/corrected sensor output and the pCO<sub>2</sub> reference,  
260 the same hereafter) are  $8.7 \pm 14.1$  μatm. pCO<sub>2,Pro</sub> shows a tight correlation with pCO<sub>2,pHTA</sub> ( $R^2 =$   
261  $0.99$ ,  $n = 29$ , not shown), and the positive correlation between  $\delta pCO_2$  and pCO<sub>2,Pro</sub> suggests an  
262 increasing offset under high pCO<sub>2</sub> conditions (Fig. 2B). This indicates that the  $\delta pCO_2$  may have  
263 been subject to a linear calibration error. When pCO<sub>2,Pro</sub> is corrected against pCO<sub>2,pHTA</sub>, the SD of  
264 the difference between the corrected sensor output (pCO<sub>2,ProCorr</sub>) and pCO<sub>2,pHTA</sub> is  $\pm 7.4$  μatm  
265 ( $\delta pCO_{2,corr}$  in Fig. 2D), which is similar to the uncertainty of pCO<sub>2,pHTA</sub> calculation ( $\pm 7.5$  μatm).  
266 There are no systematic changes in  $\delta pCO_{2,corr}$  (Fig. 2D), which suggests no other significant  
267 sources of error (i.e. biofouling, instrument drift) during the measurement. While the CO<sub>2</sub>-Pro  
268 performed very well among submersible CO<sub>2</sub> sensors in the study (ACT 2009a), the potential  
269 error in sensor measurement resulting from temperature fluctuation of the optical cell (see the PAP  
270 result section below) was not considered in the performance report by ACT (2009a).

271 ***Results of the SNOMS underway measurement***

272 The CO<sub>2</sub>-Pro units used in the SNOMS operation were factory calibrated on a yearly basis. For  
273 evaluation purposes, pCO<sub>2,Pro</sub> is compared to the pCO<sub>2,DICTA</sub> calculated from the daily DIC and TA  
274 samples, as well as to direct measurements from other pCO<sub>2</sub> measuring systems in the same region.  
275 As the pCO<sub>2</sub> measurements were intermittent at the beginning of the SNOMS project during the  
276 circumnavigation of the *MV Pacific Celebes* (2007-2009), the assessment presented below is  
277 based on the continuous measurements along the repeated transects in the Pacific (2009 onwards).  
278 From October 2009 to February 2012, the cargo ship in total made 18 transects between the  
279 western US coast, New Zealand and Australia and two CO<sub>2</sub>-Pro units were used for measurement  
280 in turn (Table 3). Of the 14 transects with successful instrumental measurements (other 2 transects  
281 failed with sensor malfunction), there are 12 transects with DIC and TA data.  
282 The difference between the raw sensor output pCO<sub>2,Pro</sub> (5-minute average corresponding to the  
283 sampling time) and pCO<sub>2,DICTA</sub> is shown in Fig. 3A. The overall offset ( $\delta pCO_2 = pCO_{2,Pro} -$   
284  $pCO_{2,DICTA}$ ) for the 12 transects is  $6.4 \pm 12.3 \mu atm$  (n=200). No correlation between  $\delta pCO_2$  and  
285 the absolute concentration of pCO<sub>2</sub> (300-500  $\mu atm$ ) is identified (not shown). It is noted that the  
286 mean and SD of  $\delta pCO_2$  vary from transect to transect (Table 3). Aside from any error and  
287 potential drift of the sensor, the difference in  $\delta pCO_2$  among transects may be caused by several  
288 other factors: 1) uncertainty in the pCO<sub>2,DICTA</sub> calculation; 2) the different responses of the two  
289 CO<sub>2</sub>-Pro units and the changing response of each unit before/after the recalibration in June 2010; 3)  
290 the influence of water patchiness, i.e. taking a discrete sample from a different water patch from  
291 that measured by the CO<sub>2</sub>-Pro as the ship travelled at a relatively high speed (~15 knots). On the  
292 other hand,  $\delta pCO_2$  values from successive transects using the same sensor generally do not differ

293 greatly (e.g. transects 2, 3, 4 for sensor 47 and transects 7, 8, 9 for sensor 48, see Table 3). The  
294 changes in  $\delta p\text{CO}_2$  among these successive transects may be mainly related to the changes in the  
295 condition of the gas transfer membranes (biofouling, contamination et al.) and the SNOMS tank  
296 (sedimentation). The values of  $\delta p\text{CO}_2$  show a random distribution around the mean value for each  
297 transect except for transects 14 and 17 (Fig. 3C, D). The  $\delta p\text{CO}_2$  in transect 14 shows a consistent  
298 increasing trend with time which may be associated with the contamination of the equilibrator or  
299 SNOMS tank (Fig. 3C). Moreover, values from the first 15 days of transect 17 (24.1  $\mu\text{atm}$ ) are  
300 significantly higher than those of the adjacent transects using the same sensor (2.6 and 7.4  $\mu\text{atm}$   
301 for transect 16 and 18 respectively), which is followed by a sudden decrease of  $\sim 40$   $\mu\text{atm}$  in  
302  $\delta p\text{CO}_2$  in the last 5 days (Fig. 3D). The causes of these dramatic changes in  $\delta p\text{CO}_2$  during this  
303 particular transect are not well identified.

304 As the calculated  $p\text{CO}_{2,\text{DICTA}}$  provides a consistent reference throughout the SNOMS operation for  
305 the two  $\text{CO}_2$ -Pro units before and after recalibration, we chose to correct  $p\text{CO}_{2,\text{Pro}}$  against  
306  $p\text{CO}_{2,\text{DICTA}}$  for each transect individually. A time-dependent correction was applied to the transect  
307 14, and the data in transect 17 are corrected in two sections as described above (Fig. 3C, D). As  
308 shown in Figure 3B, the SD of the differences between the corrected sensor outputs and  
309  $p\text{CO}_{2,\text{DICTA}}$  is  $\pm 7.8$   $\mu\text{atm}$  (Fig. 3B), which is similar to the uncertainty of the calculation of  
310  $p\text{CO}_{2,\text{DICTA}}$  ( $\pm 8.1$   $\mu\text{atm}$ ).

311 During the same period of the SNOMS transect 9, another SOO *MV Natalie Schulte* took  $p\text{CO}_2$   
312 measurement along the same route to that of the *MV Pacific Celebes*, but in a different direction  
313 (Fig. 4A). The  $p\text{CO}_2$  measuring system was operated by Pacific Marine Environmental Laboratory  
314 (PMEL), which features a showerhead design of equilibrator and NDIR detection of dried gas

315 (Pierrot et al. 2009). The availability of the regularly calibrated PMEL measurements (accuracy  
316 within  $2 \mu\text{atm}$ ) provided an opportunity for an intercomparison to evaluate the corrected SNOMS  
317  $\text{pCO}_2$  data. As shown in Figure 4, the temperature, salinity and  $\text{pCO}_2$  measured by the two  
318 systems generally display the same latitudinal distributions. The elevated  $\text{pCO}_2$  observed around  
319 the equator suggests the influence of westward advected  $\text{CO}_2$ -rich water originating from the  
320 equatorial upwelling (Fig. 4D). However, the difference in measuring time at the same location for  
321 the two ships ranges 0-16 days ( $\Delta\text{Time}$  in Fig. 4). Therefore, the difference of the two  $\text{pCO}_2$   
322 measurements (Fig. 4F) includes not only the errors of the two measurements but also the natural  
323 spatial and temporal variability of  $\text{pCO}_2$ . The latter is related to water movement and  
324 warming/cooling of the surface water, which is indicated by the temperature and salinity  
325 differences between the two datasets (Fig. 4E).

326 In order to minimize the influence of natural  $\text{pCO}_2$  variability on the comparison, the simultaneous  
327 measurements by the two systems were highlighted in Figure 5. These measurements, with a time  
328 difference less than 0.5 day, were made in the equatorial region when the two ships were within  
329 250 km of each other. The results measured by the two ships generally agreed in salinity ( $0.14 \pm$   
330  $0.05$ ) and temperature ( $0.28 \pm 0.09 \text{ }^\circ\text{C}$ , Fig. 5A). Previous time-series and Lagrangian  
331 observations in the equatorial Pacific show a diurnal  $\text{pCO}_2$  variability of 2-8  $\mu\text{atm}$ , which is  
332 mainly controlled by the temperature fluctuation (Goyet and Peltzer 1997; Degrandpre et al. 2004).

333 In order to remove the temperature effect from the  $\text{pCO}_2$  comparison, we normalize the  $\text{pCO}_{2,\text{Pro}}$  to  
334 the temperature measured by the PMEL system. When the temperature effect is removed, the  
335 SNOMS  $\text{pCO}_2$  values agree well with the PMEL measurements at  $-0.3 \pm 3.9 \mu\text{atm}$  ( $\delta\text{pCO}_2$  in Fig.  
336 5B). This indicates reasonably good accuracy of the corrected SNOMS  $\text{pCO}_2$  data (note that the



337 raw CO<sub>2</sub>-Pro outputs have been corrected against the carbonate calculation by 8.7 μatm, see Table  
338 3).

### 339 *Results of the Aquatron laboratory test*

340 As shown in Fig. 6A, the water temperature during the Aquatron test generally showed a diurnal  
341 variability of 1-3°C and it varied within 15.5-17.5°C during the intercomparison period (Fig. 6A).  
342 The evaporation-induced increase in salinity was clearly observed and a sharp salinity drop on 7  
343 August indicates the substantial addition of the fresher harbour water after drainage from the  
344 sampling tube (Fig. 6B). In order to account for the changes in chemical properties due to  
345 evaporation, DIC and TA are normalized to the mean salinity 32.3:  $nX = (X / \text{Salinity}) * 32.3$ ,  
346 where X is the measured concentration of DIC or TA, and nX is the salinity-normalized  
347 concentration (Fig. 6D). During the stabilization period, pCO<sub>2</sub> decreased from the initial value (up  
348 to 900 μatm) to a relative constant range within 640-690 μatm (Fig. 6C). At the same time, DIC  
349 and TA both showed an increasing trend (Fig. 6B) while the concentrations of nutrients remained  
350 at low levels with little variability (Fig. 6E, F). The relatively constant nDIC (~2150 μmol kg<sup>-1</sup>,  
351 Fig. 6D) suggests that the increase in DIC (Fig. 6B) mainly resulted from evaporation. In contrast,  
352 the salinity-normalized nTA increased significantly from 2240 to 2290 μmol kg<sup>-1</sup> (Fig. 6D).  
353 During the intercomparison period, the pCO<sub>2</sub> levels were adjusted to be in the “natural” open  
354 ocean range of 300-550 μatm by the bubbling of CO<sub>2</sub>-free air (started on 10 July, 2 August and 31  
355 August). Corresponding decreases in pCO<sub>2</sub> and DIC (Fig. 6B, C) were observed when the tank  
356 was purged with CO<sub>2</sub>-free air, which was followed by progressive increases after the bubbling  
357 stopped. On 7 August, the dramatic changes in all measured variables were caused by the  
358 substantial addition of newly pumped water as described above. This induced sudden decreases

359 in salinity, TA and DIC (Fig. 6A, B) that were associated with increases in pCO<sub>2</sub> and nutrients  
360 (Fig. 6C, E, F).

361 The intercomparison of the pCO<sub>2</sub> measurements by the SNOMS and NOIZ systems is presented in  
362 Figure 7. The CO<sub>2</sub>-Pro functioned properly throughout the Aquatron test while the NOIZ system  
363 suffered from malfunctions on a few occasions (the failed measurements are not included in the  
364 intercomparison, Fig. 7A). Both measurements were averaged to 5 minute interval and pCO<sub>2,NOIZ</sub>  
365 was normalized to the temperature in the SNOMS tank to eliminate temperature influence on the  
366 comparison (the average temperature difference is ~0.08 °C, which corresponds to ~1.5 µatm in  
367 pCO<sub>2</sub>). There may be a slight delay in pCO<sub>2,Pro</sub> when responding to the pCO<sub>2</sub> disturbances  
368 (bubbling, water top up) as these events occurred in the Aquatron tank were first observed by the  
369 NOIZ system. Overall, the pCO<sub>2</sub> measured by the two systems shows a tight correlation (pCO<sub>2,Pro</sub>  
370 = 0.9987 \* pCO<sub>2,NOIZ</sub>, R<sup>2</sup> = 0.99, not shown). The mean and SD of the differences between the  
371 two measurements ( $\delta pCO_2 = pCO_{2,Pro} - pCO_{2,NOIZ}$ ) are  $-3.0 \pm 4.4$  µatm (n = 13847, Fig. 7C).  
372  $\delta pCO_2$  does not show a constant drift over the two month test (Fig. 7C) but appears to vary with  
373 the absolute pCO<sub>2</sub> concentration (Fig. 7B), which may be due to a linear error in the sensor  
374 calibration. When the CO<sub>2</sub>-Pro measurements are calibrated against pCO<sub>2,NOIZ</sub>, the differences  
375 between the calibrated pCO<sub>2,ProCorr</sub> and pCO<sub>2,NOIZ</sub> ( $\delta pCO_{2,corr}$  in Fig. 7D,  $0 \pm 2.9$  µatm) show a  
376 random distribution around the mean value throughout the intercomparison experiment, which  
377 suggests no instrumental drift of the CO<sub>2</sub>-Pro occurred during the two-month period.

378 An interesting phenomenon observed in the Aquatron test is the unexpected changes in alkalinity.  
379 The increase in nTA during the stabilization period (2240 to 2290 µmol kg<sup>-1</sup>, Fig. 6D) cannot be  
380 explained by the changes in inorganic carbon content and nutrients: (1) the small changes in nDIC

381 and nutrients indicate minor TA changes resulted from biological activities such as precipitation  
382 and dissolution of  $\text{CaCO}_3$  (which changes TA and DIC at a ratio of 2:1) and nutrient uptake and  
383 release by algae (which changes TA following the nutrient- $\text{H}^+$ -compensation principle)  
384 (Wolf-Gladrow et al. 2007); (2) air-sea gas exchange of  $\text{CO}_2$  changes DIC but does not affect the  
385 concentration of TA (Wolf-Gladrow et al. 2007); (3) the oxygen saturation varied between 86-104%  
386 (not shown) which suggests no TA changes induced by anaerobic processes. Similarly, increases  
387 in nTA observed after the top up event on 7 August (2270 to 2290  $\mu\text{mol kg}^{-1}$ ) also did not match  
388 the changes in nDIC and nitrates: the increasing concentrations of nDIC and nitrates during this  
389 period (Fig. 6D, E) suggests the occurrence of remineralization processes which would decrease  
390 TA.

391 In order to examine the TA anomaly in the Aquatron test, we calculate alkalinity from the  
392 measured DIC and  $\text{pCO}_2$  using the CO2SYS. The calculated  $\text{Alk}_{\text{sys}}$  (uncertainty estimated to be  $\pm$   
393 3.5  $\mu\text{mol kg}^{-1}$ ) is the alkalinity expected at the equilibration state of the carbonate system, which  
394 accounts for the major inorganic buffering acid-base pairs. It is shown in Figure 8A that the  
395 concentrations of  $\text{Alk}_{\text{sys}}$  are 3-24  $\mu\text{mol kg}^{-1}$  lower than the measured values of  $\text{TA}_{\text{meas}}$ . This excess  
396 of  $\text{TA}_{\text{meas}}$  over the  $\text{Alk}_{\text{sys}}$  ( $\text{Alk}_{\text{excess}}$ ) suggests substances or processes which affect the  
397 concentration of alkalinity and/or the titration process of alkalinity. This may be due to: waste  
398 water or reactive particles in the harbour, contamination during the pumping process, reaction  
399 with the fibreglass wall of the Aquatron tank, or the existence of organic alkalinity. Although we  
400 cannot clearly identify the source(s) of the alkalinity anomaly, it is shown that using the measured  
401  $\text{TA}_{\text{meas}}$  for carbonate calculation would result in underestimates in  $\text{pCO}_2$  (Fig. 8B). The  $\text{pCO}_{2,\text{DICTA}}$   
402 calculated from  $\text{TA}_{\text{meas}}$  and DIC is 7-90  $\mu\text{atm}$  lower compared to the direct  $\text{pCO}_2$  measurement,

403 and this underestimation ( $p\text{CO}_{2,\text{bias}} = p\text{CO}_{2,\text{Pro}} - p\text{CO}_{2,\text{DICTA}}$ ) shows a similar trend to that of  
404  $\text{Alk}_{\text{excess}}$  (Fig. 8C). Closer investigation shows that the percentage bias in  $p\text{CO}_2$  ( $\%p\text{CO}_{2,\text{bias}} =$   
405  $p\text{CO}_{2,\text{bias}} / p\text{CO}_{2,\text{Pro}}$ ) is positively correlated to the percentage bias in alkalinity ( $\%\text{Alk}_{\text{excess}} =$   
406  $\text{Alk}_{\text{excess}} / \text{TA}_{\text{meas}} = 12.54 * \%p\text{CO}_{2,\text{bias}}$ , Fig. 8D).

#### 407 ***Results of the long-term in situ operation on the PAP mooring***

408 Since the first deployment in June 2010, a  $\text{CO}_2$ -Pro continuously worked at the PAP site until  
409 January 2011 when a communication cable of the hub controller broke. A calibrated unit replaced  
410 the original sensor in July 2011 and operated until March 2012 when the controlling hub was  
411 flooded. A frustratingly short deployment during May to July 2012 was due to communication  
412 failure when the sensor frame became detached from the mooring. The deployment of the  
413  $\text{CO}_2$ -Pro at PAP was successful for up to 7 months while the failure of longer measurement was  
414 due to problems of the hub controller rather than the sensor malfunction.

415 In contrast to continuous measurement on SOO, the  $\text{CO}_2$ -Pro on the PAP mooring was operated  
416 intermittently (1-4 times a day) due to the limited power supply. Each measurement lasted for  
417 45-120 minutes which assures full equilibrium with the seawater (typically within 15 minutes).  
418 The  $p\text{CO}_2$  of the oligotrophic surface water around the PAP site is expected to show minor  
419 variability during the short duration of each measurement. However, the  $p\text{CO}_2$  measured by the  
420  $\text{CO}_2$ -Pro showed a consistent increase throughout each measurement (Fig. 9A presents a typical  
421 measuring cycle of the  $\text{CO}_2$ -Pro) while the in situ temperature and salinity remained unchanged  
422 (not shown). It is noted that the optical cell temperature of the detector shows an increasing trend  
423 similar to that of  $p\text{CO}_2$  (Fig. 9A). Moreover, the cell temperature during the measurement ( $t_{\text{meas}}$ ) is  
424 found to be much higher than that during the ZPC ( $\Delta t_{\text{cell}} = t_{\text{meas}} - t_{\text{ZPC}}$ , Fig. 9A). As the NDIR

425 measurement is affected by the optical cell temperature, this temperature fluctuation would result  
426 in errors in pCO<sub>2</sub> detection.

427 In order to examine the influence of optical cell temperature, a laboratory test was carried out  
428 when the sensor was recovered from deployment. A series of CO<sub>2</sub> standard gases (256, 363 and  
429 459 ppm) were connected to the detector bypassing the equilibrator for direct NDIR  
430 measurements. In addition, a CO<sub>2</sub>-free gas (N<sub>2</sub> passing through CO<sub>2</sub> absorbance) was used to  
431 simulate the baseline measurement of C<sub>zero</sub> during the ZPC. Measurements of these gases  
432 were carried out following a ZPC at 40 °C, while the temperature of the optical cell during the  
433 measurement of each gas was perturbed by heating with an electric breeze and cooling with a  
434 cold pack ( $\Delta t_{\text{cell}}$  was adjusted to be -0.7 to 1.8 °C). The test results show that the inferred  
435 signals of all measured gases decrease linearly with increasing optical cell temperature (not  
436 shown). As the zero-CO<sub>2</sub> signal also changes with temperature, using a baseline measured at  
437  $t_{\text{zero}}$  as the blank reference for measurements at different cell temperatures would result in  
438 errors in calculating  $\epsilon$  and xCO<sub>2</sub>. As shown in Figure 9B, the errors in xCO<sub>2</sub> ( $x\text{CO}_{2,\text{error}} =$   
439 measured xCO<sub>2</sub> – certified value) were linearly correlated with  $\Delta t_{\text{cell}}$ , and the temperature  
440 effects are similar for the three standard gases at 15 ppm °C<sup>-1</sup>. It is also shown that the errors  
441 in xCO<sub>2</sub> can be removed if the influence of  $\Delta t_{\text{cell}}$  is considered in the calculations of  $\epsilon$  and  
442 xCO<sub>2</sub> (Fig. 9B). The scatter of the data should mainly be caused by the uneven heating or  
443 cooling on the optical cell in our test.

444 When this correction of  $\Delta t_{\text{cell}}$  is applied to the PAP measurement, the corrected pCO<sub>2,tcorr</sub>  
445 stabilizes at 15 minutes after the ZPC as expected from the equilibrium time and shows minor  
446 changes afterward (Fig. 9A). It is notable that the  $\Delta t_{\text{cell}}$  at the PAP mooring is quite large (up

447 to 1.5 °C), which corresponds to an error in pCO<sub>2</sub> as large as 25 µatm. This is because of the  
448 early ZPC at low t<sub>ZPC</sub> when the optical cell was not sufficiently warmed up, as well as  
449 inadequate thermostat control of the optical cell, i.e. the cell temperature continued to  
450 increase after the ZPC. In contrast, this issue is not significant for the continuous  
451 measurements as the long-term operation allows the optical cell to be fully warmed up  
452 minimizing the temperature difference between ZPC and measurement. The Δt<sub>cell</sub> during the  
453 SNOMS and Aquatron operations was ~ 0.2 °C corresponding to an error of 3 µatm in pCO<sub>2</sub>;  
454 corrections of Δt<sub>cell</sub> are applied to the SNOMS and Aquatron data before assessment.

#### 455 **Discussion, recommendations and improvements**

456 Overall, the CO<sub>2</sub>-Pro is a very robust sensor suitable for onboard and in situ measurements on  
457 platforms with limited working space and on platforms that cannot be serviced regularly. The  
458 sensor's capacity for long-term operation is demonstrated by the successes of the SNOMS  
459 operation and PAP mooring deployments. In this study, the performance of the CO<sub>2</sub>-Pro is  
460 evaluated extensively under field and laboratory conditions and the results are summarized in  
461 Table 4. The CO<sub>2</sub>-Pro agreed with a calibrated water-air equilibrator system during a 2-month  
462 side-by-side laboratory intercomparison ( $-3.0 \pm 4.4$  µatm). When used at sea, the direct sensor  
463 outputs differed from the calculated pCO<sub>2</sub> reference by  $6.4 \pm 12.3$  µatm on a SOO and  $8.7 \pm 14.1$   
464 µatm on a mooring. These differences result from a number of factors including the uncertainties  
465 in the reference and the comparison process, the sensor error, how well the sensor was set up,  
466 contamination issues etc. Our study suggests that, when pCO<sub>2</sub> references are available for  
467 correction, the uncertainty of the corrected sensor result is similar to and largely determined by the  
468 uncertainties of the references.

469 One significant limitation of the CO<sub>2</sub>-Pro is the lack of regular calibration against standard gases,  
470 which makes it difficult to assess the accuracy of the measurement when it is deployed alone. To  
471 remedy this potential problem, Pro-Oceanus has introduced a new version of CO<sub>2</sub>-Pro with  
472 on-board control of a gas port for introduction of standard gases. If the CO<sub>2</sub>-Pro is to be used for  
473 onboard or laboratory measurements, this version which enables external manual calibration is  
474 recommended to be used. In the future, an automatic calibration function using standard gases  
475 would be highly desired to optimize the accuracy of the measurement. For the field  
476 applications, users of the CO<sub>2</sub>-Pro (and any chemical sensor that is not calibrated while deployed)  
477 should calibrate the sensor before and after long-term deployments to examine any potential drift.  
478 Collection of discrete samples over a wide range of pCO<sub>2</sub> concentrations for the determination of  
479 other carbonate variables is recommended to provide quality control on the sensor, and also, to  
480 provide additional information on biogeochemical variability.

481 Clearly, the accuracy of the calibration gases used in the original factory calibration and any  
482 subsequent recalibrations is a critical factor in sensor accuracy. However, this study reveals  
483 that some inaccuracy of the sensor may be caused by calibration error which may be related to  
484 the quality of calibration gases used. To address this problem, Pro-Oceanus has performed all  
485 factory calibrations using NOAA and NOAA traceable standard gases that are accurate to  
486 better than  $\pm 1$  ppm since 2011. Moreover, our study reveals that error in pCO<sub>2</sub> measurement of  
487 the CO<sub>2</sub>-Pro can result from the changes in optical cell temperature between the ZPC and  
488 measurement. This problem may be significant for the early versions of CO<sub>2</sub>-Pro whose optical  
489 cells are not well thermostatically controlled. However, this error is correctable and can be  
490 avoided by better temperature control on the detector optical cell. Since 2011, an improved

491 temperature control is a standard feature of CO<sub>2</sub>-Pro which stabilizes the fluctuation of the  
492 temperature of the detector cell to within  $\pm 0.05$  °C.

493 In order to fulfil the target of constraining the regional air-sea CO<sub>2</sub> fluxes to 0.2 Pg C year<sup>-1</sup>, pCO<sub>2</sub>  
494 measuring systems need to be accurate to within 2  $\mu$ atm for seawater pCO<sub>2</sub> (Pierrot et al. 2009).  
495 This is presently a demanding requirement for pCO<sub>2</sub> sensors. As demonstrated in this work, the  
496 CO<sub>2</sub>-Pro sensors that were tested (particularly the older versions) did not meet the gold standard of  
497 2  $\mu$ atm. However, recent improvements to the CO<sub>2</sub>-Pro (as mentioned above) should enhance  
498 sensor performance. Considering the large variability of pCO<sub>2</sub> in time and space, there is great  
499 value in expanding in situ observations by using sensors with a known reasonably good accuracy.

500 The developing sensor technology provides a very effective way to increase the capability for  
501 global and regional ocean monitoring. This can provide useful information on the surface ocean  
502 where no or few measurements have been made or other extreme marine environments such as in  
503 the deep ocean (the CO<sub>2</sub>-Pro has been successfully used on the SeaCycler and NEPTUNE  
504 profilers, Johnson, B personal communication) or near hydrothermal vents (Nakano et al. 2006;  
505 Willcox et al. 2009). Moreover, the long-term time series data from fixed-station sensor  
506 deployments provides a most powerful tool to understand the controlling mechanisms regulating  
507 the changes in ocean CO<sub>2</sub>.

508 Another interesting finding in this study is the alkalinity anomaly and the mismatch in carbonate  
509 calculation in the Aquatron test. Excess of measured TA (up to 24  $\mu$ mol kg<sup>-1</sup>) are found in  
510 comparison to that calculated from DIC and pCO<sub>2</sub>, while the carbonate calculation of pCO<sub>2</sub> using  
511 measured TA and DIC result in underestimation in pCO<sub>2</sub> (up to 90  $\mu$ atm). Although the causes of  
512 this TA anomaly cannot be confirmed in our study, one possible explanation is the organic



513 contribution to alkalinity. Many previous studies have proved the existent of organic alkalinity in  
514 both laboratory cultures (up to 800  $\mu\text{mol kg}^{-1}$ ) and natural coastal environments (tens of  $\mu\text{mol kg}^{-1}$ )  
515 (Cai et al. 1998; Hernandez-Ayon et al. 2007; Muller and Bleie 2008; Kim and Lee 2009). Since  
516 the use of alkalinity including organic bases could lead to errors in the carbonate calculation, care  
517 should be taken when making calculations for the marine carbonate system in environments with  
518 high concentration of organic matter, e.g. estuary, coastal water and incubation culture solution.  
519 When studying the organic matter-rich waters, alkalinity is recommended to be measured using  
520 method proposed by Cai et al. (1998) or Hernández-Ayón et al. (1999) to identify the organic  
521 alkalinity.

522

523 **Reference**

- 524 ACT. 2009a. Performance demonstration statement Pro-Oceanus Systems Inc. PSI CO<sub>2</sub>-Pro™.  
525 Alliance for Coastal Technologies, report Ref.No. ACT TD10-03.
- 526 ---. 2009b. Protocols for demonstrating the performance of in situ pCO<sub>2</sub> analyzers. Alliance  
527 for Coastal Technologies, report Ref.No. ACT PD09-01.
- 528 Bakker, D. C. E. and others (2013) An update to the Surface Ocean CO<sub>2</sub> Atlas (SOCAT  
529 version 2). Earth System Science Data Discussions, 6, 465–512,  
530 doi:10.5194/essdd-6-465-2013.
- 531 Bates, N. R. 2002. Seasonal variability of the effect of coral reefs on seawater CO<sub>2</sub> and air-sea  
532 CO<sub>2</sub> exchange. *Limnol. Oceanogr.* **47**: 43-52.
- 533 ---. 2007. Interannual variability of the oceanic CO<sub>2</sub> sink in the subtropical gyre of the North  
534 Atlantic Ocean over the last 2 decades. *J. Geophys. Res.* **112**: C09013.
- 535 Beggs, H. M., R. Verein, G. Paltoglou, H. Kippo, and M. Underwood. 2012. Enhancing ship  
536 of opportunity sea surface temperature observations in the Australian region. *J. Oper.*  
537 *Oceanogr.* **5**: 59-73.
- 538 Borges, A. V., and M. Frankignoulle. 1999. Daily and seasonal variations of the partial  
539 pressure of CO<sub>2</sub> in surface seawater along Belgian and southern Dutch coastal areas. *J.*  
540 *Mar. Syst.* **19**: 251-266.
- 541 Cai, W. J., Y. C. Wang, and R. E. Hodson. 1998. Acid-base properties of dissolved organic  
542 matter in the estuarine waters of Georgia, USA. *Geochim. Cosmochim. Acta* **62**:  
543 473-483.
- 544 Dai, M. H. and others 2009. Diurnal variations of surface seawater pCO<sub>2</sub> in contrasting  
545 coastal environments. *Limnol. Oceanogr.* **54**: 735-745.
- 546 De La Paz, M., A. Gomez-Parra, and J. Forja. 2008. Tidal-to-seasonal variability in the  
547 parameters of the carbonate system in a shallow tidal creek influenced by  
548 anthropogenic inputs, Rio San Pedro (SW Iberian Peninsula). *Cont. Shelf Res.* **28**:  
549 1394-1404.
- 550 Degrandpre, M. D. 1993. Measurement of seawater pCO<sub>2</sub> using a renewable-reagent fiber  
551 optic sensor with colorimetric detection. *Anal. Chem.* **65**: 331-337.
- 552 Degrandpre, M. D., M. M. Baehr, and T. R. Hammar. 1999. Calibration-free optical chemical  
553 sensors. *Anal. Chem.* **71**: 1152-1159.
- 554 Degrandpre, M. D., T. R. Hammar, S. P. Smith, and F. L. Sayles. 1995. In situ measurements  
555 of seawater pCO<sub>2</sub>. *Limnol. Oceanogr.* **40**: 969-975.
- 556 Degrandpre, M. D., T. R. Hammar, and C. D. Wirick. 1998. Short-term pCO<sub>2</sub> and O<sub>2</sub>  
557 dynamics in California coastal waters. *Deep Sea Res., Part II* **45**: 1557-1575.
- 558 Degrandpre, M. D., R. Wanninkhof, W. R. Mcgillis, and P. G. Strutton. 2004. A Lagrangian  
559 study of surface pCO<sub>2</sub> dynamics in the eastern equatorial Pacific Ocean. *J. Geophys.*  
560 *Res.* **109**: C08S07.
- 561 Dickson, A. G. 1990. Standard potential of the (AgCl(s)+½ H<sub>2</sub>(g) = Ag(s) + HCl(aq)) cell and  
562 the dissociation constant of bisulfate ion in synthetic sea water from 273.15 to 318.15  
563 K. *J. Chem. Thermodyn.* **22**: 113-127.

564 Dickson, A. G., C. L. Sabine, and J. R. Christian (2007), *Guide to best practices for ocean*  
565 *CO<sub>2</sub> measurements*, 191 pp., North Pacific Marine Science Organization (PICES),  
566 Sidney, British Columbia.

567 Doney, S. C. and others 2009. Surface-ocean CO<sub>2</sub> variability and vulnerability. *Deep Sea Res.*,  
568 Part II **56**: 504-511.

569 Fiedler, B., P. Fietzek, N. Vieira, P. Silva, H. C. Bittig, and A. Körtzinger. 2012. In situ CO<sub>2</sub>  
570 and O<sub>2</sub> measurements on a profiling float. *J. Atmos. Oceanic Technol.* **30**: 112-126.

571 Goyet, C., and E. T. Peltzer. 1997. Variation of CO<sub>2</sub> partial pressure in surface seawater in the  
572 equatorial Pacific Ocean. *Deep Sea Res.*, Part I **44**: 1611-1625.

573 Goyet, C., D. R. Walt, and P. G. Brewer. 1992. Development of a fiber optic sensor for  
574 measurement of pCO<sub>2</sub> in sea water: design criteria and sea trials. *Deep Sea Res.*, Part  
575 I **39**: 1015-1026.

576 Hartman, S. E. and others 2012. The Porcupine Abyssal Plain fixed-point sustained  
577 observatory (PAP-SO): variations and trends from the Northeast Atlantic fixed-point  
578 time-series. *ICES J. Mar. Sci.* **69**: 776-783.

579 Hernandez-Ayon, J. M., A. Zirino, A. G. Dickson, T. Camiro-Vargas, and E.  
580 Valenzuela-Espinoza. 2007. Estimating the contribution of organic bases from  
581 microalgae to the titration alkalinity in coastal seawaters. *Limnol. Oceanogr. Methods*  
582 **5**: 225-232.

583 Hernández-Ayón, J. M. N., S. L. Belli, and A. Zirino. 1999. pH, alkalinity and total CO<sub>2</sub> in  
584 coastal seawater by potentiometric titration with a difference derivative readout. *Anal.*  
585 *Chim. Acta* **394**: 101-108.

586 Hydes, D. J. and others 2013. Report of the SNOMS Project 2006 to 2012, SNOMS: SWIRE  
587 NOCS Ocean Monitoring System. Part 1: Narrative description. National  
588 Oceanography Centre Research and Consultancy Report, 33.

589 Jiang, Z.-P. and others 2011. Short-term dynamics of oxygen and carbon in productive  
590 nearshore shallow seawater systems off Taiwan: Observations and modeling. *Limnol.*  
591 *Oceanogr.* **56**: 1832-1849.

592 Jiang, Z.-P. and others 2013. Key controls on the seasonal and interannual variations of the  
593 carbonate system and air-sea CO<sub>2</sub> flux in the Northeast Atlantic (Bay of Biscay). *J.*  
594 *Geophys. Res.* **118**: 1-16.

595 Kayanne, H. and others 2002. Submersible system to measure seawater pCO<sub>2</sub> on a shallow  
596 sea floor. *Mar. Technol. Soc. J.* **36**: 23-28.

597 Kim, H.-C., and K. Lee. 2009. Significant contribution of dissolved organic matter to  
598 seawater alkalinity. *Geophys. Res. Lett.* **36**: L20603.

599 Körtzinger, A., H. Thomas, B. Schneider, N. Gronau, L. Mintrop, and J. C. Duinker. 1996.  
600 At-sea intercomparison of two newly designed underway pCO<sub>2</sub> systems -  
601 encouraging results. *Mar. Chem.* **52**: 133-145.

602 Lee, S. S., C. Park, P. Fenter, N. C. Sturchio, and K. L. Nagy. 2010. Competitive adsorption  
603 of strontium and fulvic acid at the muscovite-solution interface observed with  
604 resonant anomalous X-ray reflectivity. *Geochim. Cosmochim. Acta* **74**: 1762-1776.

605 Lefèvre, N., J. P. Ciabrini, G. Michard, B. Brient, M. Duchaffaut, and L. Merlivat. 1993. A  
606 new optical sensor for pCO<sub>2</sub> measurement. *Mar. Chem.*: 189-198.

607 Lu, Z., M. Dai, K. Xu, J. Chen, and Y. Liao. 2008. A high precision, fast response, and low  
608 power consumption in situ optical fiber chemical pCO<sub>2</sub> sensor. *Talanta* **76**: 353-359.  
609 doi: 310.1016/j.talanta.2008.1003.1005.

610 Mehrbach, C., C. H. Culberson, J. E. Hawley, and R. M. Pytkowicz. 1973. Measurement of  
611 the apparent dissociation constants of carbonic acid in seawater at atmospheric  
612 pressure. *Limnol. Oceanogr.* **18**: 897-907.

613 Millero, F. J., T. B. Graham, F. Huang, H. Bustos-Serrano, and D. Pierrot. 2006. Dissociation  
614 constants of carbonic acid in seawater as a function of salinity and temperature. *Mar.*  
615 *Chem.* **100**: 80-94.

616 Mojica Prieto, F. J., and F. J. Millero. 2002. The values of pK<sub>1</sub> + pK<sub>2</sub> for the dissociation of  
617 carbonic acid in seawater. *Geochim. Cosmochim. Acta* **66**: 2529-2540.

618 Muller, F. L. L., and B. Bleie. 2008. Estimating the organic acid contribution to coastal  
619 seawater alkalinity by potentiometric titrations in a closed cell. *Anal. Chim. Acta* **619**:  
620 183-191.

621 Nakano, Y., H. Kimoto, S. Watanabe, K. Harada, and Y. W. Watanabe. 2006. Simultaneous  
622 vertical measurements of in situ pH and CO<sub>2</sub> in the sea using spectrophotometric  
623 profilers. *J. Oceanogr.* **62**: 71-81.

624 Nemoto, K. and others 2009. Continuous observations of atmospheric and oceanic CO<sub>2</sub> using  
625 a moored buoy in the East China Sea: Variations during the passage of typhoons.  
626 *Deep Sea Res., Part II* **56**: 542-553.

627 Pierrot, D., E. Lewis, and D. W. R. Wallace. 2006. MS Excel program developed for CO<sub>2</sub>  
628 system calculations. ORNL/CDIAC-105a. Carbon Dioxide Information Analysis  
629 Center, Oak Ridge National Laboratory, US Department of Energy, Oak Ridge, TN.

630 Pierrot, D. and others 2009. Recommendations for autonomous underway pCO<sub>2</sub> measuring  
631 systems and data-reduction routines. *Deep Sea Res., Part II* **56**: 512-522.

632 Rubin, S. I., and H. Ping Wu. 2000. A novel fiber-optic sensor for the long-term, autonomous  
633 measurement of pCO<sub>2</sub> in seawater, p. 631-639 vol.631. OCEANS 2000 MTS/IEEE  
634 Conference and Exhibition.

635 Saderne, V., P. Fietzek, and P. M. J. Herman. 2013. Extreme Variations of pCO<sub>2</sub> and pH in a  
636 Macrophyte Meadow of the Baltic Sea in Summer: Evidence of the Effect of  
637 Photosynthesis and Local Upwelling. *PLoS ONE* **8**: e62689.

638 Shitashima, K. 2010. Evolution of compact electrochemical in-situ pH-pCO<sub>2</sub> sensor using  
639 ISFET-pH electrode, p. 1-4. OCEANS 2010.

640 Tabacco, M. B., M. Uttamial, M. Mcallister, and D. R. Walt. 1999. An autonomous sensor  
641 and telemetry system for low-level pCO<sub>2</sub> measurements in seawater. *Anal. Chem.* **71**:  
642 1483-1483.

643 Takahashi, T., J. Olafsson, J. G. Goddard, D. W. Chipman, and S. C. Sutherland. 1993.  
644 Seasonal variation of CO<sub>2</sub> and nutrients in the high-latitude surface ocean: a  
645 comparative study. *Global Biogeochem. Cycles* **7**: 843-878.

646 Takahashi, T. and others 2009. Climatological mean and decadal change in surface ocean  
647 pCO<sub>2</sub>, and net sea-air CO<sub>2</sub> flux over the global oceans. *Deep-Sea Res., Pt II* **56**:  
648 554-577.

649 Thomas, H., and B. Schneider. 1999. The seasonal cycle of carbon dioxide in Baltic Sea  
650 surface waters. *J. Mar. Syst.* **22**: 53-67.

- 651 Turk, D., J. W. Book, and W. R. Mcgillis. 2013.  $p\text{CO}_2$  and  $\text{CO}_2$  exchange during high bora  
652 winds in the Northern Adriatic. *J. Mar. Syst.* **117–118**: 65-71.
- 653 Turk, D., V. Malačić, M. D. Degrandpre, and W. R. Mcgillis. 2010. Carbon dioxide  
654 variability and air-sea fluxes in the northern Adriatic Sea. *J. Geophys. Res.* **115**:  
655 C10043.
- 656 Wang, Z. A., W. J. Cai, Y. C. Wang, and B. L. Upchurch. 2003. A long pathlength liquid-core  
657 waveguide sensor for real-time  $p\text{CO}_2$  measurements at sea. *Mar. Chem.* **84**: 73-84.
- 658 Wang, Z. H., Y. H. Wang, W. J. Cai, and S. Y. Liu. 2002. A long pathlength  
659 spectrophotometric  $p\text{CO}_2$  sensor using a gas-permeable liquid-core waveguide.  
660 *Talanta* **57**: 69-80.
- 661 Watson, A. J. and others 2009. Tracking the variable North Atlantic sink for atmospheric  $\text{CO}_2$ .  
662 *Science* **326**: 1391-1393.
- 663 Whitlege, T. E., S. C. Malloy, C. J. Patton, and C. O. Wirick. 1981. Automated nutrient  
664 analysis in seawater. Brookhaven National Lab Report 51398: 216.
- 665 Willcox, S. and others 2009. An autonomous mobile platform for underway surface carbon  
666 measurements in open-ocean and coastal waters, p. 1-8. OCEANS 2009, MTS/IEEE  
667 Biloxi - Marine Technology for Our Future: Global and Local Challenges.
- 668 Wolf-Gladrow, D. A., R. E. Zeebe, C. Klaas, A. Kortzinger, and A. G. Dickson. 2007. Total  
669 alkalinity: The explicit conservative expression and its application to biogeochemical  
670 processes. *Mar. Chem.* **106**: 287-300.
- 671 Yates, K. K., C. Dufore, N. Smiley, C. Jackson, and R. B. Halley. 2007. Diurnal variation of  
672 oxygen and carbonate system parameters in Tampa Bay and Florida Bay. *Mar. Chem.*  
673 **104**: 110-124.
- 674 Zeebe, R. E., and D. Wolf-Gladrow (2001), *CO<sub>2</sub> in Seawater: Equilibrium, Kinetics, Isotopes.*,  
675 356 pp., Elsevier, Amsterdam.

Table 1 The various designs of pCO<sub>2</sub> sensors

Equilibrator	Measured phase	Determination	References
direct contact of water-gas	gas	NDIR	ACT (2009a); Nemoto et al. (2009)
gas permeable interface	gas	NDIR	Kayanne et al. (2002); Fiedler et al. (2012); Saderne et al. (2013), this study
gas permeable interface	indicator solution	electrode	Shitashima 2010
gas permeable interface	indicator solution	fluorescence	Goyet et al. (1992); Tabacco et al. (1999); Rubin and Ping Wu (2000)
gas permeable interface	indicator solution	spectrophotometry	Degradpre (1993); Lefèvre et al. (1993); Degradpre et al. (1995; 1999); Wang et al. (2002; 2003); Nakano et al. (2006); Lu et al. (2008)

Table 2 The estimated uncertainties of the pCO<sub>2</sub> (µatm) calculated from various inputs (pH and TA, or DIC and TA) in this study

	Measured pCO <sub>2</sub>	Sources of uncertainty in pCO <sub>2</sub> calculation				Uncertainty of the calculated pCO <sub>2</sub>
		pK <sub>1</sub> , pK <sub>2</sub>	TA	DIC	pH	
ACT	280 to 840	4 to 12	0.5		6.8	7.5
SNOMS	300 to 500	7 to 10	2.3	3.8		8.1
Aquatron	280 to 860	6 to 15	4.4	6.6		9.9

Table 3 The mean and standard deviation (SD) of the differences in the CO<sub>2</sub>-Pro outputs (pCO<sub>2,Pro</sub>) and those calculated from DIC and TA (pCO<sub>2,DICTA</sub>) during the SNOMS operation in the Pacific. R<sup>2</sup> refer to the correlation coefficients and *n* is the number of the pairs of pCO<sub>2</sub>.

No.	Start port	End port	Start date	End date	Sensor	pCO <sub>2,Pro</sub> - pCO <sub>2,DICTA</sub>	SD	R <sup>2</sup>	n
1	Taranga	Vancouver	23-Oct-09	11-Nov-09	48	5.7	9.8	0.91	14
2	Vancouver	Brisbane	02-Dec-09	25-Dec-09	48	failed measurement			
3	Taranga	Los Angeles	29-Jan-10	18-Feb-10	47	8.3	9.9	0.92	18
4	Los Angeles	Wellington	27-Mar-10	13-Apr-10	47	16.9	4.5	0.98	14
5	Taranga	Los Angeles	14-May-10	02-Jun-10	47	12.0	8.2	0.94	16
6	Vancouver	Auckland	25-Jun-10	14-Jul-10	48	failed measurement			
7	Taranga	Los Angeles	18-Aug-10	07-Sep-10	48	-6.6	8.6	0.97	19
8	Los Angeles	Brisbane	05-Oct-10	25-Oct-10	48	5.9	6.1	0.98	20
9	Taranga	Los Angeles	21-Nov-10	12-Dec-10	48	8.7	7.5	0.98	15
10	Los Angeles	Brisbane	18-Jan-11	12-Feb-11	none	no measurement; system removed for calibration			
11	Taranga	Los Angeles	16-Mar-11	10-Apr-11	none	no measurement; system removed for calibration			
12	Los Angeles	Brisbane	05-May-11	25-May-11	recalibrated 47	successful measurement; no DIC and TA data			
13	Taranga	Los Angeles	15-Jun-11	06-Jul-11	recalibrated 47	successful measurement; no DIC and TA data			
14	Los Angeles	Brisbane	30-Jul-11	20-Aug-11	recalibrated 47	0.3	18.0	0.85	18
15	Taranga	Los Angeles	20-Sep-11	09-Oct-11	recalibrated 47	6.6	8.3	0.94	15
16	Los Angeles	Brisbane	09-Nov-11	29-Nov-11	recalibrated 48	2.6	11.3	0.92	19
17	Taranga	Los Angeles	03-Jan-12	17-Jan-12	recalibrated 48	24.1	5.1	0.99	14
			18-Jan-12	23-Jan-12	recalibrated 48	-15.57 (sudden drop)	10.1		5
18	Los Angeles	Taranga	11-Feb-12	29-Feb-12	recalibrated 48	7.4	7.4	0.94	14

Table 4 Summary of the assessment results of the CO<sub>2</sub>-Pro in this study

	Application	Mode	Time length	Reference and its uncertainty	Difference with the reference ( $\mu\text{atm}$ )	
					direct output	corrected output
ACT	mooring test	in situ	16-day	calculation from pH and TA ( $\pm 7.5 \mu\text{atm}$ )	$8.7 \pm 14.1$	$0 \pm 7.4$
SNOMS	SOO observation	underway	several months	calculation from DIC and TA ( $\pm 8.1 \mu\text{atm}$ )	$6.4 \pm 12.3$	$0.2 \pm 7.8$
				direct and calibrated measurement ( $\pm 2 \mu\text{atm}$ )		$-0.3 \pm 3.9$
Aquatron	laboratory test	underway	2 months	direct and calibrated measurement ( $\pm 2 \mu\text{atm}$ )	$-3.0 \pm 4.4$	$0 \pm 2.9$



## Figure Captions:

Fig. 1 Schematic of the flow paths of the ProOceanus CO<sub>2</sub>-Pro<sup>TM</sup> pCO<sub>2</sub> sensor. See the text for details.

Fig. 2 The results of the ACT test in Kaneohe Bay: (A) the continuously hourly pCO<sub>2,Pro</sub> from the CO<sub>2</sub>-Pro and the pCO<sub>2,pHTA</sub> calculated from discrete pH and TA; (B) the correlation between the  $\delta pCO_2$  ( $\delta pCO_2 = pCO_{2,Pro} - pCO_{2,pHTA}$ ) and pCO<sub>2,Pro</sub>, the linear fit and the 95% prediction bands are shown; (C)  $\delta pCO_2$  ( $8.4 \pm 14.1 \mu atm$ ) vs. time; (D)  $\delta pCO_{2,corr} = pCO_{2,ProCorr} - pCO_{2,pHTA}$  ( $0 \pm 7.4 \mu atm$ ) vs. time, where pCO<sub>2,ProCorr</sub> is the sensor output corrected by pCO<sub>2,pHTA</sub> using the regression shown in panel B. Figure adapted from ACT (2009a).

Fig. 3 For the 12 Pacific transects during the SNOMS operation, (A)  $\delta pCO_2 = pCO_{2,Pro} - pCO_{2,DICTA}$ , where pCO<sub>2,Pro</sub> is the raw sensor output and pCO<sub>2,DICTA</sub> is calculated from DIC and TA, the mean and SD of  $\delta pCO_2$  are  $6.4 \pm 12.3 \mu atm$ ; (B)  $\delta pCO_{2,corr} = pCO_{2,ProCorr} - pCO_{2,DICTA}$ , where pCO<sub>2,ProCorr</sub> is the pCO<sub>2,Pro</sub> corrected by pCO<sub>2,pHTA</sub> for individual transects, the mean and SD of  $\delta pCO_{2,corr}$  are  $0.2 \pm 7.8 \mu atm$ . The increasing  $\delta pCO_2$  in transect 14 and the sudden changes in  $\delta pCO_2$  in transect 17 are shown in panel (C) and (D), together with the  $\delta pCO_{2,corr}$ .

Fig. 4 (A) The overlapping route of the two ships of opportunity; the latitudinal distributions of (B) salinity, (C) SST, (D) pCO<sub>2</sub> measured by the PMEL and SNOMS systems; and their differences in (E) SST, salinity and (F) pCO<sub>2</sub>.  $\Delta Time$  is the difference in measuring time at the same location for the two ships.

Fig. 5 The differences of the simultaneous measurements (time difference less than 0.5 day and distance within 250 km) by the SNOMS and PMEL systems: (A) SST and salinity; (B) pCO<sub>2</sub>.

Fig. 6 The variations of (A) temperature and salinity, (B) DIC and TA, (C) pCO<sub>2</sub> measured by the CO<sub>2</sub>-Pro and the NOIZ system, (D) salinity normalized nDIC and nTA, (E) nitrate and phosphate, and (F) silicate and ammonia during the Aquatron test. The dashed line and the solid line correspond to the starting of the intercomparison and the substantial water top up event respectively. The arrow lines in panel (C) correspond to the starting of the bubbling of the CO<sub>2</sub>-free gas. See the text for details.

Fig. 7 The results of the two-month intercomparison between the CO<sub>2</sub>-Pro and the calibrated NOIZ system: (A) pCO<sub>2</sub>; (B) the pCO<sub>2</sub> differences ( $\delta pCO_2 = pCO_{2,Pro} - pCO_{2,NOIZ}$ ) vs. pCO<sub>2,NOIZ</sub>, the linear fit and the 95% prediction bands are shown; (C)  $\delta pCO_2$  vs. time; (D)  $\delta pCO_{2,corr}$  is the pCO<sub>2</sub> differences between the corrected pCO<sub>2,Pro</sub> and pCO<sub>2,NOIZ</sub>.

Fig. 8 (A) The concentrations of TA<sub>meas</sub> from direct measurement and Alk<sub>sys</sub> calculated from the measured DIC and pCO<sub>2</sub>; (B) pCO<sub>2</sub> measured by the CO<sub>2</sub>-Pro (pCO<sub>2,Pro</sub>) and pCO<sub>2,DICTA</sub> calculated from the measured DIC and TA; (C) the differences of TA and pCO<sub>2</sub> between direct measurements and the carbonate calculations ( $Alk_{excess} = TA_{meas} - Alk_{sys}$ ,  $pCO_{2,bias} = pCO_{2,Pro} - pCO_{2,DICTA}$ ); (D) the correlation between the percentage of pCO<sub>2,bias</sub> and Alk<sub>excess</sub> in comparison to the measured values ( $\% pCO_{2,bias} = pCO_{2,bias} / pCO_{2,Pro}$ ,  $\% Alk_{excess} = Alk_{excess} / TA_{meas}$ ).

Fig. 9 (A) A typical measuring cycle of the CO<sub>2</sub>-Pro on PAP mooring,  $\Delta t_{cell}$  is the optical cell temperature deviation during the measurement in compared to that during the zero point calibration, pCO<sub>2,raw</sub> and pCO<sub>2,tcorr</sub> are the raw sensor outputs and those corrected for the influence of  $\Delta t_{cell}$ ; (B) the errors in xCO<sub>2</sub> measurements resulting from  $\Delta t_{cell}$  for the three standard gases in the laboratory test, and those after correction for the temperature influence. See the text for details.

the laboratory test, and those after correction for the temperature influence. See the text for details.

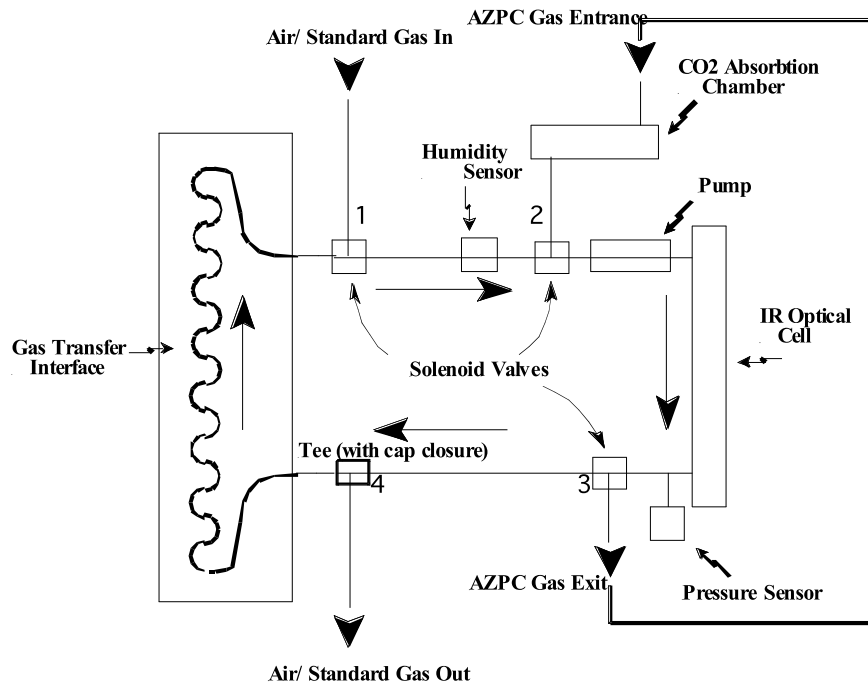


Fig. 1 Schematic of the flow paths of the ProOceanus CO<sub>2</sub>-Pro™ pCO<sub>2</sub> sensor. See the text for details.

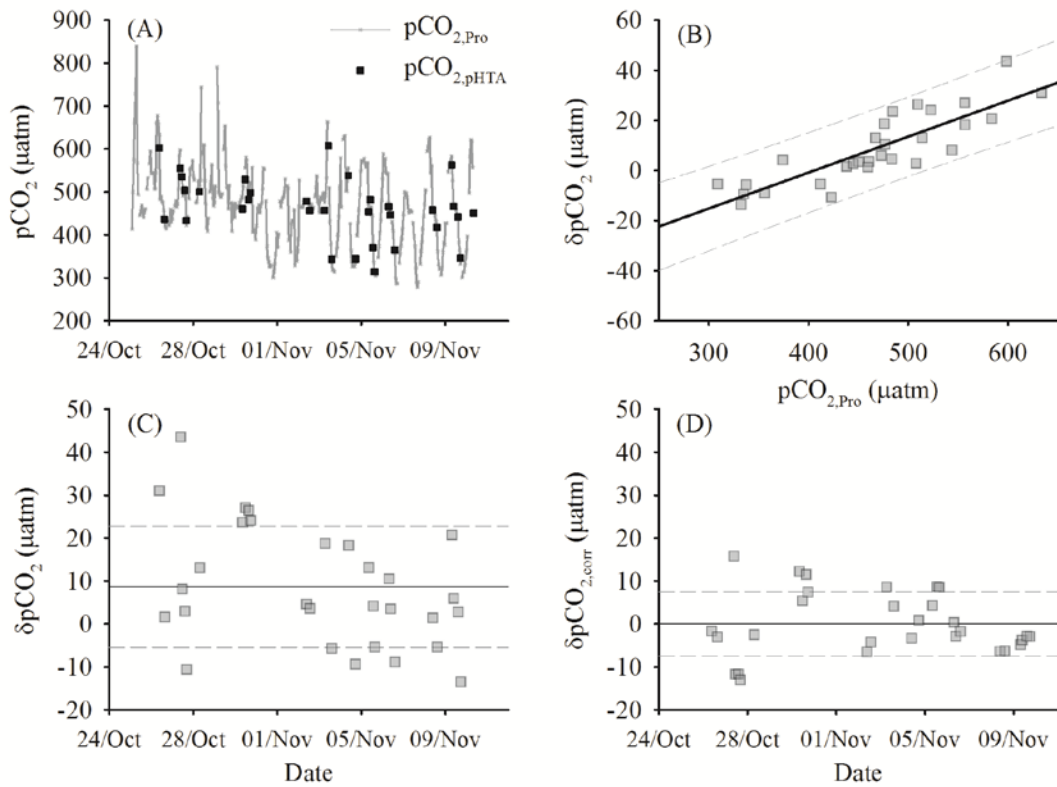


Fig. 2 The results of the ACT test in Kaneohe Bay: (A) the continuously hourly pCO<sub>2,Pro</sub> from the CO<sub>2</sub>-Pro and the pCO<sub>2,pHTA</sub> calculated from discrete pH and TA; (B) the correlation between the δpCO<sub>2</sub> ( $\delta pCO_2 = pCO_{2,Pro} - pCO_{2,pHTA}$ ) and pCO<sub>2,Pro</sub>, the linear fit and the 95% prediction bands are shown; (C) δpCO<sub>2</sub> ( $8.4 \pm 14.1 \mu\text{atm}$ ) vs. time; (D) δpCO<sub>2,corr</sub> = pCO<sub>2,ProCorr</sub> - pCO<sub>2,pHTA</sub> ( $0 \pm 7.4 \mu\text{atm}$ ) vs. time, where pCO<sub>2,ProCorr</sub> is the sensor output corrected by pCO<sub>2,pHTA</sub> using the regression shown in panel B. Figure adapted from ACT (2009a).

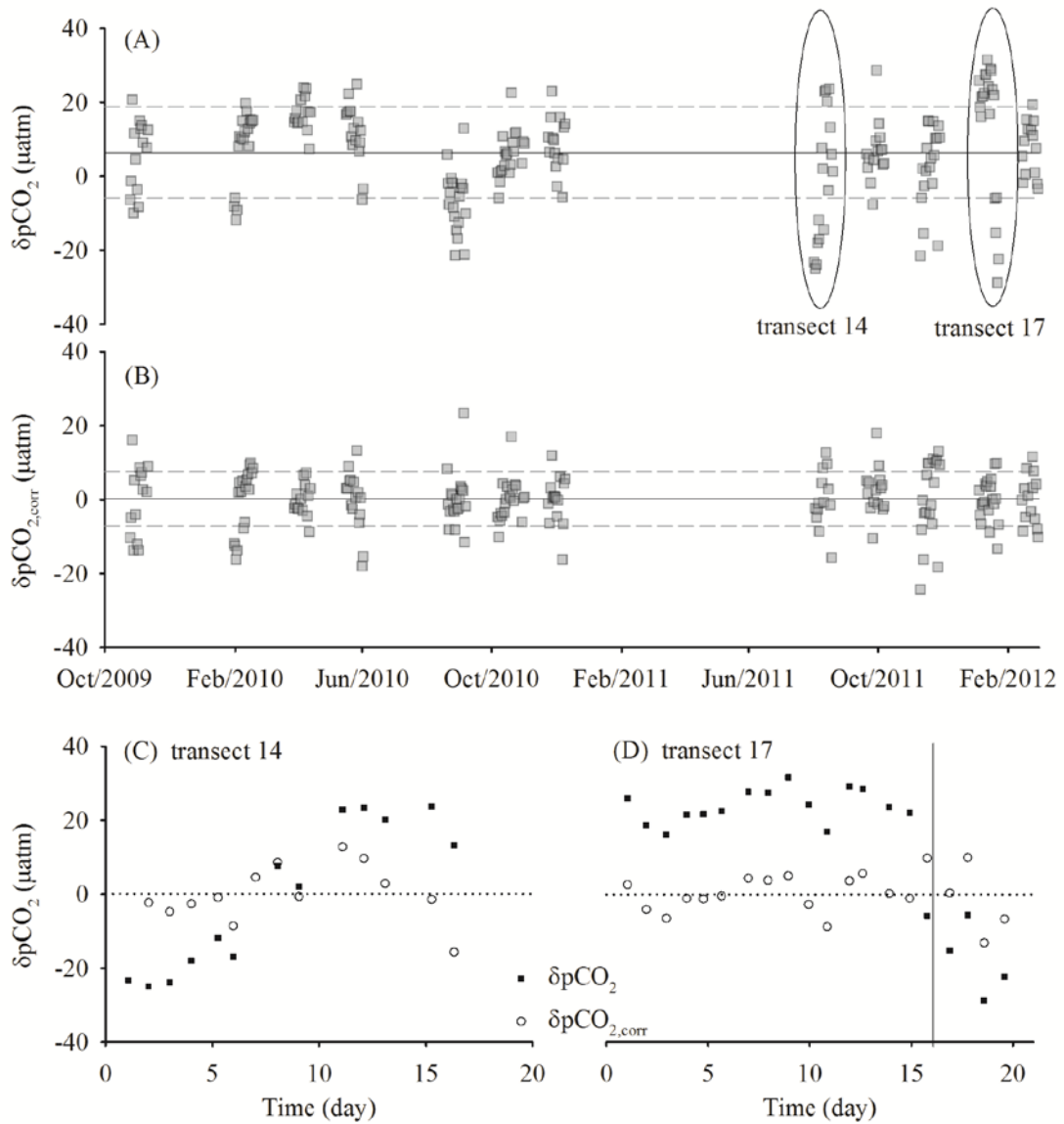


Fig. 3 For the 12 Pacific transects during the SNOMS operation, (A)  $\delta p\text{CO}_2 = p\text{CO}_{2,\text{Pro}} - p\text{CO}_{2,\text{DICTA}}$ , where  $p\text{CO}_{2,\text{Pro}}$  is the raw sensor output and  $p\text{CO}_{2,\text{DICTA}}$  is calculated from DIC and TA, the mean and SD of  $\delta p\text{CO}_2$  are  $6.4 \pm 12.3 \mu\text{atm}$ ; (B)  $\delta p\text{CO}_{2,\text{corr}} = p\text{CO}_{2,\text{ProCorr}} - p\text{CO}_{2,\text{DICTA}}$ , where  $p\text{CO}_{2,\text{ProCorr}}$  is the  $p\text{CO}_{2,\text{Pro}}$  corrected by  $p\text{CO}_{2,\text{pHTA}}$  for individual transects, the mean and SD of  $\delta p\text{CO}_{2,\text{corr}}$  are  $0.2 \pm 7.8 \mu\text{atm}$ . The increasing  $\delta p\text{CO}_2$  in transect 14 and the sudden changes in  $\delta p\text{CO}_2$  in transect 17 are shown in panel (C) and (D), together with the  $\delta p\text{CO}_{2,\text{corr}}$ .

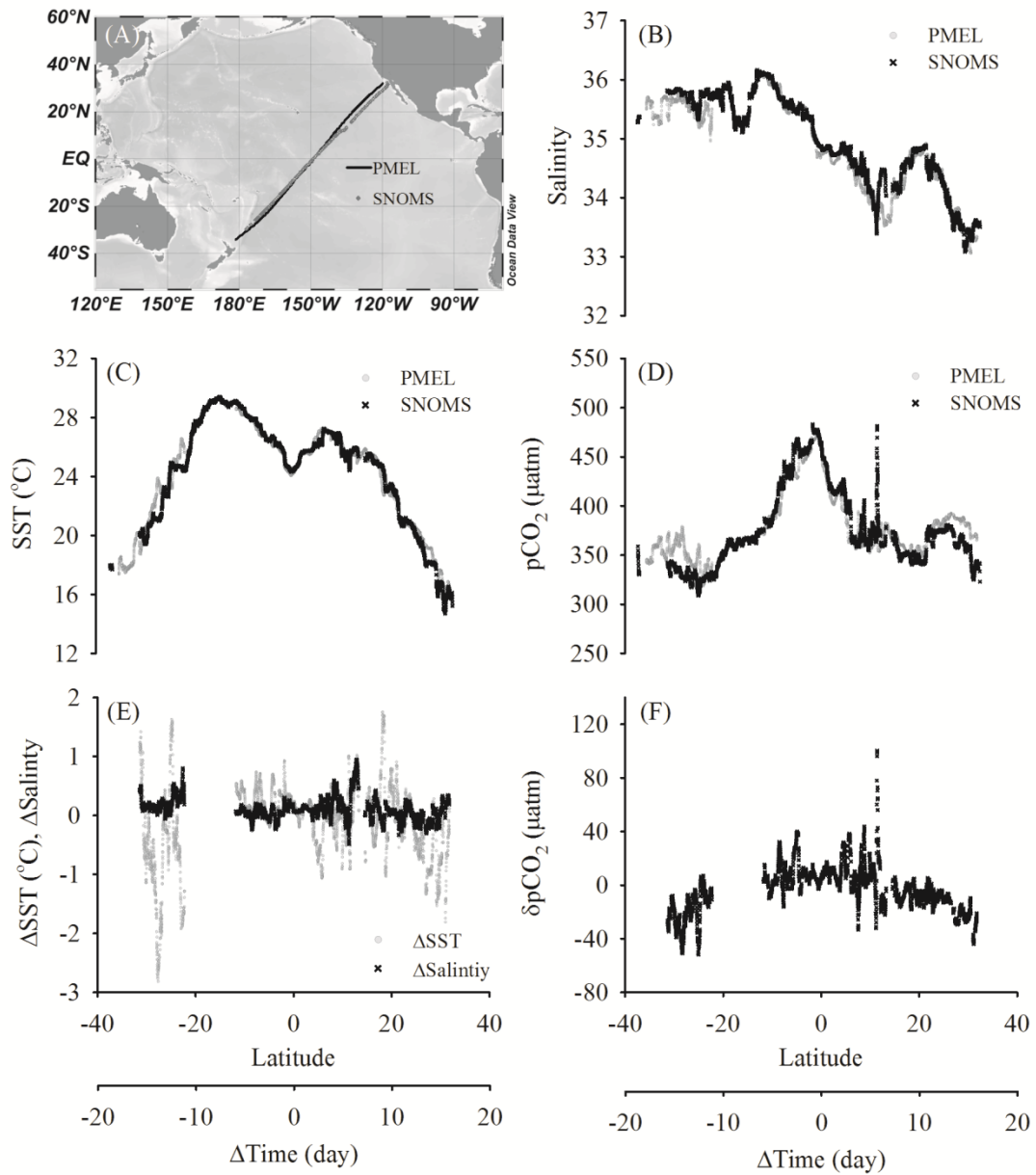


Fig. 4 (A) The overlapping route of the two ships of opportunity; the latitudinal distributions of (B) salinity, (C) SST, (D) pCO<sub>2</sub> measured by the PMEL and SNOMS systems; and their differences in (E) SST, salinity and (F) pCO<sub>2</sub>. ΔTime is the difference in measuring time at the same location for the two ships.

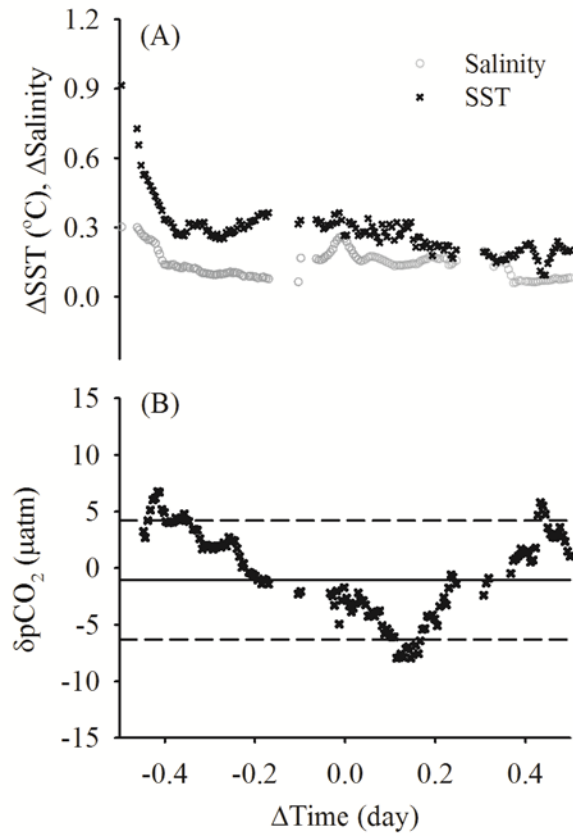


Fig. 5 The differences of the simultaneous measurements (time difference less than 0.5 day and distance within 250 km) by the SNOMS and PMEL systems: (A) SST and salinity; (B)  $\text{pCO}_2$ .

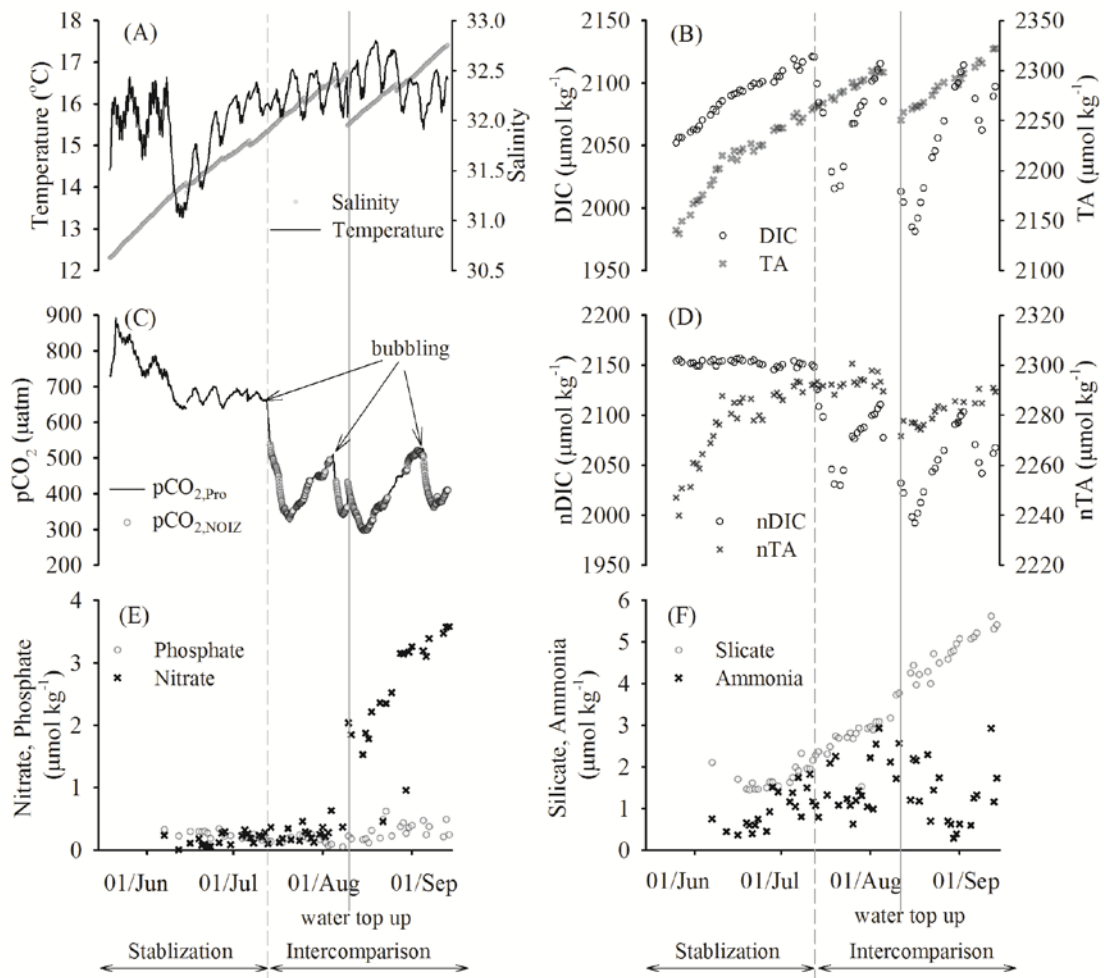


Fig. 6 The variations of (A) temperature and salinity, (B) DIC and TA, (C)  $p\text{CO}_2$  measured by the  $\text{CO}_2$ -Pro and the NOIZ system, (D) salinity normalized nDIC and nTA, (E) nitrate and phosphate, and (F) silicate and ammonia during the Aquatron test. The dashed line and the solid line correspond to the starting of the intercomparison and the substantial water top up event respectively. The arrow lines in panel (C) correspond to the starting of the bubbling of the  $\text{CO}_2$ -free gas. See the text for details.



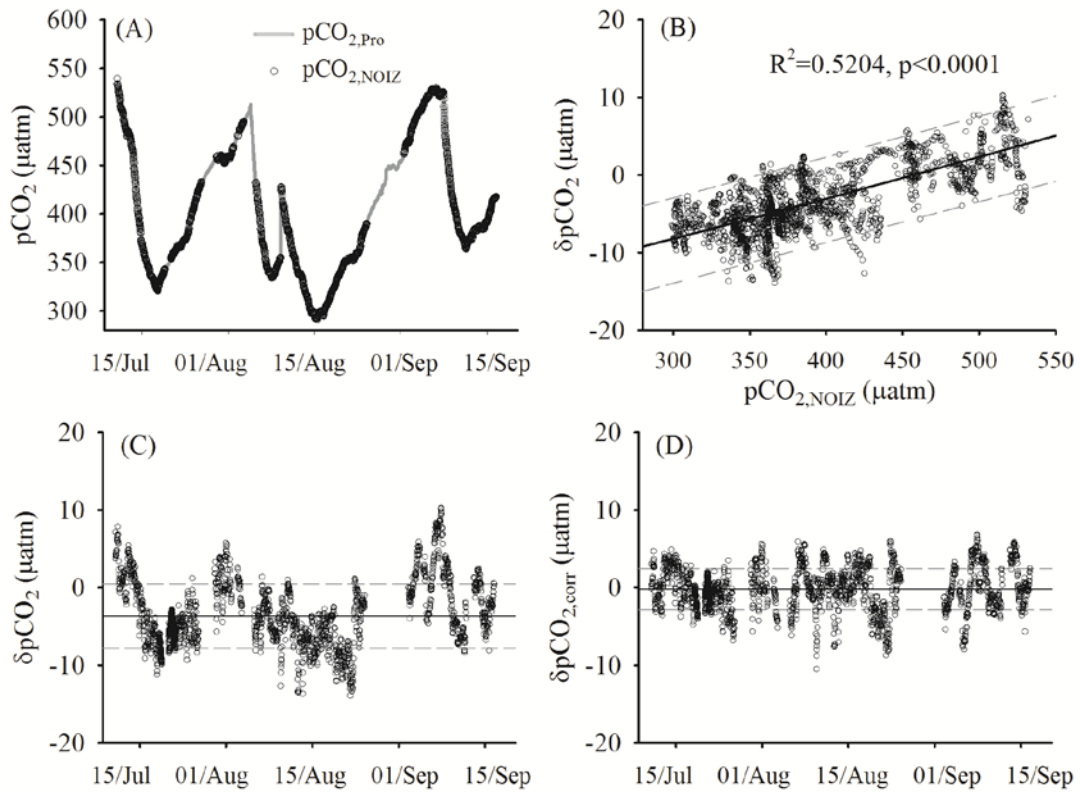


Fig. 7 The results of the two-month intercomparison between the CO<sub>2</sub>-Pro and the calibrated NOIZ system: (A) pCO<sub>2</sub>; (B) the pCO<sub>2</sub> differences ( $\delta pCO_2 = pCO_{2,Pro} - pCO_{2,NOIZ}$ ) vs. pCO<sub>2,NOIZ</sub>, the linear fit and the 95% prediction bands are shown; (C)  $\delta pCO_2$  vs. time; (D)  $\delta pCO_{2,corr}$  is the pCO<sub>2</sub> differences between the corrected pCO<sub>2,Pro</sub> and pCO<sub>2,NOIZ</sub>.

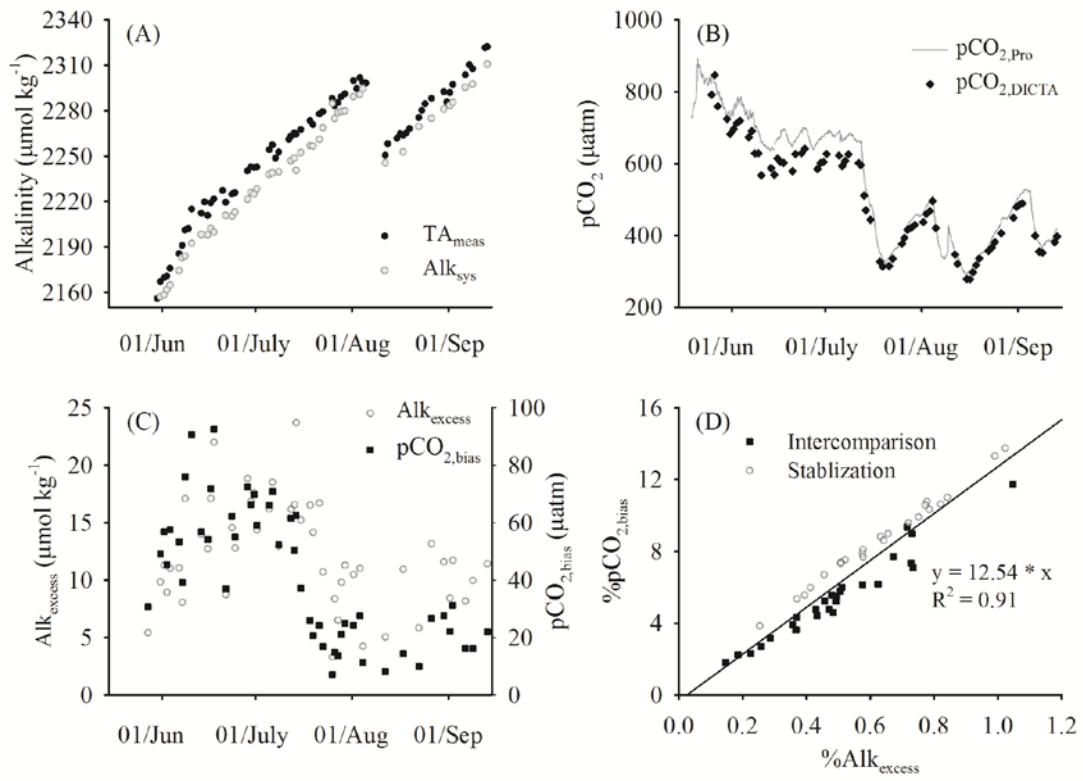


Fig. 8 (A) The concentrations of  $\text{TA}_{\text{meas}}$  from direct measurement and  $\text{Alk}_{\text{sys}}$  calculated from the measured DIC and  $\text{pCO}_2$ ; (B)  $\text{pCO}_2$  measured by the  $\text{CO}_2$ -Pro ( $\text{pCO}_{2,\text{Pro}}$ ) and  $\text{pCO}_{2,\text{DICTA}}$  calculated from the measured DIC and TA; (C) the differences of TA and  $\text{pCO}_2$  between direct measurements and the carbonate calculations ( $\text{Alk}_{\text{excess}} = \text{TA}_{\text{meas}} - \text{Alk}_{\text{sys}}$ ,  $\text{pCO}_{2,\text{bias}} = \text{pCO}_{2,\text{Pro}} - \text{pCO}_{2,\text{DICTA}}$ ); (D) the correlation between the percentage of  $\text{pCO}_{2,\text{bias}}$  and  $\text{Alk}_{\text{excess}}$  in comparison to the measured values ( $\% \text{pCO}_{2,\text{bias}} = \text{pCO}_{2,\text{bias}} / \text{pCO}_{2,\text{Pro}}$ ,  $\% \text{Alk}_{\text{excess}} = \text{Alk}_{\text{excess}} / \text{TA}_{\text{meas}}$ ).

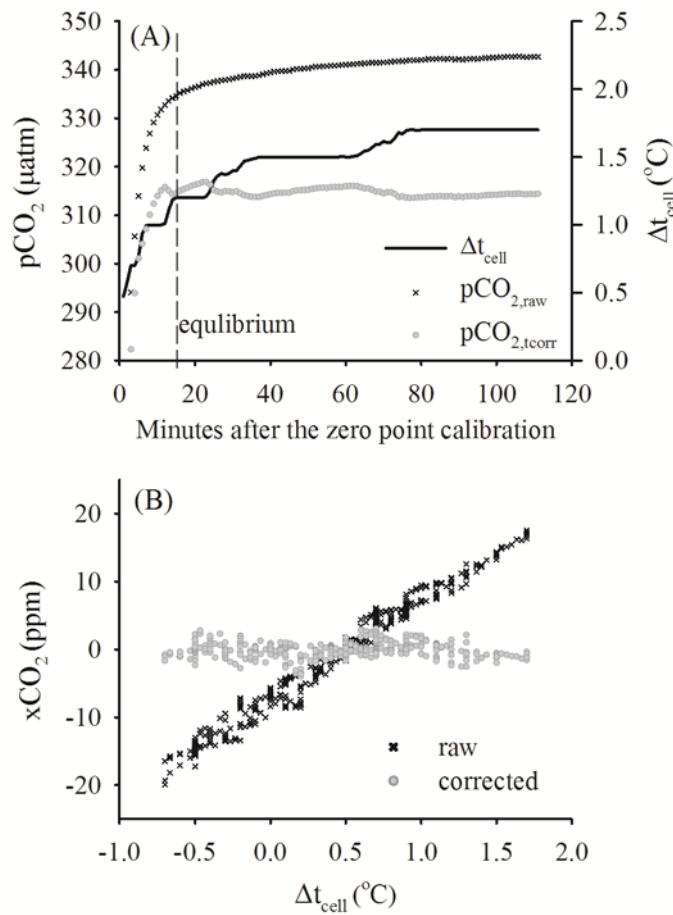


Fig. 9 (A) A typical measuring cycle of the CO<sub>2</sub>-Pro on PAP mooring, Δt<sub>cell</sub> is the optical cell temperature deviation during the measurement in compared to that during the zero point calibration, pCO<sub>2,raw</sub> and pCO<sub>2,tcorr</sub> are the raw sensor outputs and those corrected for the influence of Δt<sub>cell</sub>; (B) the errors in xCO<sub>2</sub> measurements resulting from Δt<sub>cell</sub> for the three standard gases in the laboratory test, and those after correction for the temperature influence. See the text for details.